



**IJOER**  
RESEARCH JOURNAL

ISSN

2395-6992

# International Journal of Engineering Research & Science

[www.ijoer.com](http://www.ijoer.com)

[www.adpublications.org](http://www.adpublications.org)

Volume-9! Issue-10! October, 2023

[www.ijoer.com](http://www.ijoer.com) ! [info@ijoer.com](mailto:info@ijoer.com)

## Preface

We would like to present, with great pleasure, the inaugural volume-9, Issue-10, October 2023, of a scholarly journal, *International Journal of Engineering Research & Science*. This journal is part of the AD Publications series *in the field of Engineering, Mathematics, Physics, Chemistry and science Research Development*, and is devoted to the gamut of Engineering and Science issues, from theoretical aspects to application-dependent studies and the validation of emerging technologies.

This journal was envisioned and founded to represent the growing needs of Engineering and Science as an emerging and increasingly vital field, now widely recognized as an integral part of scientific and technical investigations. Its mission is to become a voice of the Engineering and Science community, addressing researchers and practitioners in below areas

Chemical Engineering	
Biomolecular Engineering	Materials Engineering
Molecular Engineering	Process Engineering
Corrosion Engineering	
Civil Engineering	
Environmental Engineering	Geotechnical Engineering
Structural Engineering	Mining Engineering
Transport Engineering	Water resources Engineering
Electrical Engineering	
Power System Engineering	Optical Engineering
Mechanical Engineering	
Acoustical Engineering	Manufacturing Engineering
Optomechanical Engineering	Thermal Engineering
Power plant Engineering	Energy Engineering
Sports Engineering	Vehicle Engineering
Software Engineering	
Computer-aided Engineering	Cryptographic Engineering
Teletraffic Engineering	Web Engineering
System Engineering	
Mathematics	
Arithmetic	Algebra
Number theory	Field theory and polynomials
Analysis	Combinatorics
Geometry and topology	Topology
Probability and Statistics	Computational Science
Physical Science	Operational Research
Physics	
Nuclear and particle physics	Atomic, molecular, and optical physics
Condensed matter physics	Astrophysics
Applied Physics	Modern physics
Philosophy	Core theories

Chemistry	
Analytical chemistry	Biochemistry
Inorganic chemistry	Materials chemistry
Neurochemistry	Nuclear chemistry
Organic chemistry	Physical chemistry
Other Engineering Areas	
Aerospace Engineering	Agricultural Engineering
Applied Engineering	Biomedical Engineering
Biological Engineering	Building services Engineering
Energy Engineering	Railway Engineering
Industrial Engineering	Mechatronics Engineering
Management Engineering	Military Engineering
Petroleum Engineering	Nuclear Engineering
Textile Engineering	Nano Engineering
Algorithm and Computational Complexity	Artificial Intelligence
Electronics & Communication Engineering	Image Processing
Information Retrieval	Low Power VLSI Design
Neural Networks	Plastic Engineering

Each article in this issue provides an example of a concrete industrial application or a case study of the presented methodology to amplify the impact of the contribution. We are very thankful to everybody within that community who supported the idea of creating a new Research with IJOER. We are certain that this issue will be followed by many others, reporting new developments in the Engineering and Science field. This issue would not have been possible without the great support of the Reviewer, Editorial Board members and also with our Advisory Board Members, and we would like to express our sincere thanks to all of them. We would also like to express our gratitude to the editorial staff of AD Publications, who supported us at every stage of the project. It is our hope that this fine collection of articles will be a valuable resource for *IJOER* readers and will stimulate further research into the vibrant area of Engineering and Science Research.



Mukesh Arora  
(Chief Editor)

## **Board Members**

### **Mr. Mukesh Arora (Editor-in-Chief)**

BE (Electronics & Communication), M.Tech (Digital Communication), currently serving as Assistant Professor in the Department of ECE.

### **Prof. Dr. Fabricio Moraes de Almeida**

Professor of Doctoral and Master of Regional Development and Environment - Federal University of Rondonia.

### **Dr. Parveen Sharma**

Dr Parveen Sharma is working as an Assistant Professor in the School of Mechanical Engineering at Lovely Professional University, Phagwara, Punjab.

### **Prof. S. Balamurugan**

Department of Information Technology, Kalaingar Karunanidhi Institute of Technology, Coimbatore, Tamilnadu, India.

### **Dr. Omar Abed Elkareem Abu Arqub**

Department of Mathematics, Faculty of Science, Al Balqa Applied University, Salt Campus, Salt, Jordan, He received PhD and Msc. in Applied Mathematics, The University of Jordan, Jordan.

### **Dr. AKPOJARO Jackson**

Associate Professor/HOD, Department of Mathematical and Physical Sciences, Samuel Adegboyega University, Ogwa, Edo State.

### **Dr. Ajoy Chakraborty**

Ph.D.(IIT Kharagpur) working as Professor in the department of Electronics & Electrical Communication Engineering in IIT Kharagpur since 1977.

### **Dr. Ukar W. Soelistijo**

Ph D, Mineral and Energy Resource Economics, West Virginia State University, USA, 1984, retired from the post of Senior Researcher, Mineral and Coal Technology R&D Center, Agency for Energy and Mineral Research, Ministry of Energy and Mineral Resources, Indonesia.

### **Dr. Samy Khalaf Allah Ibrahim**

PhD of Irrigation &Hydraulics Engineering, 01/2012 under the title of: "Groundwater Management under Different Development Plans in Farafra Oasis, Western Desert, Egypt".

### **Dr. Ahmet ÇİFCİ**

Ph.D. in Electrical Engineering, Currently Serving as Head of Department, Burdur Mehmet Akif Ersoy University, Faculty of Engineering and Architecture, Department of Electrical Engineering.

## **Dr. M. Varatha Vijayan**

Annauniversity Rank Holder, Commissioned Officer Indian Navy, Ncc Navy Officer (Ex-Serviceman Navy), Best Researcher Awardee, Best Publication Awardee, Tamilnadu Best Innovation & Social Service Awardee From Lions Club.

## **Dr. Mohamed Abdel Fatah Ashabrawy Moustafa**

PhD. in Computer Science - Faculty of Science - Suez Canal University University, 2010, Egypt.

Assistant Professor Computer Science, Prince Sattam bin AbdulAziz University ALkharj, KSA.

## **Prof.S.Balamurugan**

Dr S. Balamurugan is the Head of Research and Development, Quants IS & CS, India. He has authored/co-authored 35 books, 200+ publications in various international journals and conferences and 6 patents to his credit. He was awarded with Three Post-Doctoral Degrees - Doctor of Science (D.Sc.) degree and Two Doctor of Letters (D.Litt) degrees for his significant contribution to research and development in Engineering.

## **Dr. Mahdi Hosseini**

Dr. Mahdi did his Pre-University (12<sup>th</sup>) in Mathematical Science. Later he received his Bachelor of Engineering with Distinction in Civil Engineering and later he Received both M.Tech. and Ph.D. Degree in Structural Engineering with Grade "A" First Class with Distinction.

## **Dr. Anil Lamba**

Practice Head – Cyber Security, EXL Services Inc., New Jersey USA.

Dr. Anil Lamba is a researcher, an innovator, and an influencer with proven success in spearheading Strategic Information Security Initiatives and Large-scale IT Infrastructure projects across industry verticals. He has helped bring about a profound shift in cybersecurity defense. Throughout his career, he has parlayed his extensive background in security and a deep knowledge to help organizations build and implement strategic cybersecurity solutions. His published researches and conference papers has led to many thought provoking examples for augmenting better security.

## **Dr. Ali İhsan KAYA**

Currently working as Associate Professor in Mehmet Akif Ersoy University, Turkey.

**Research Area:** Civil Engineering - Building Material - Insulation Materials Applications, Chemistry - Physical Chemistry – Composites.

## **Dr. Parsa Heydarpour**

Ph.D. in Structural Engineering from George Washington University (Jan 2018), GPA=4.00.

## **Dr. Heba Mahmoud Mohamed Afify**

Ph.D degree of philosophy in Biomedical Engineering, Cairo University, Egypt worked as Assistant Professor at MTI University.

### **Dr. Aurora Angela Pisano**

Ph.D. in Civil Engineering, Currently Serving as Associate Professor of Solid and Structural Mechanics (scientific discipline area nationally denoted as ICAR/08—"Scienza delle Costruzioni"), University Mediterranea of Reggio Calabria, Italy.

### **Dr. Faizullah Mahar**

Associate Professor in Department of Electrical Engineering, Balochistan University Engineering & Technology Khuzdar. He is PhD (Electronic Engineering) from IQRA University, Defense View, Karachi, Pakistan.

### **Prof. Viviane Barrozo da Silva**

Graduated in Physics from the Federal University of Paraná (1997), graduated in Electrical Engineering from the Federal University of Rio Grande do Sul - UFRGS (2008), and master's degree in Physics from the Federal University of Rio Grande do Sul (2001).

### **Dr. S. Kannadhasan**

Ph.D (Smart Antennas), M.E (Communication Systems), M.B.A (Human Resources).

### **Dr. Christo Ananth**

Ph.D. Co-operative Networks, M.E. Applied Electronics, B.E Electronics & Communication Engineering Working as Associate Professor, Lecturer and Faculty Advisor/ Department of Electronics & Communication Engineering in Francis Xavier Engineering College, Tirunelveli.

### **Dr. S.R.Boselin Prabhu**

Ph.D, Wireless Sensor Networks, M.E. Network Engineering, Excellent Professional Achievement Award Winner from Society of Professional Engineers Biography Included in Marquis Who's Who in the World (Academic Year 2015 and 2016). Currently Serving as Assistant Professor in the department of ECE in SVS College of Engineering, Coimbatore.

### **Dr. PAUL P MATHAI**

Dr. Paul P Mathai received his Bachelor's degree in Computer Science and Engineering from University of Madras, India. Then he obtained his Master's degree in Computer and Information Technology from Manonmanium Sundaranar University, India. In 2018, he received his Doctor of Philosophy in Computer Science and Engineering from Noorul Islam Centre for Higher Education, Kanyakumari, India.

### **Dr. M. Ramesh Kumar**

Ph.D (Computer Science and Engineering), M.E (Computer Science and Engineering).

Currently working as Associate Professor in VSB College of Engineering Technical Campus, Coimbatore.

### **Dr. Maheshwar Shrestha**

Postdoctoral Research Fellow in DEPT. OF ELE ENGG & COMP SCI, SDSU, Brookings, SD Ph.D, M.Sc. in Electrical Engineering from SOUTH DAKOTA STATE UNIVERSITY, Brookings, SD.

### **Dr. D. Amaranatha Reddy**

Ph.D. (Postdoctoral Fellow, Pusan National University, South Korea), M.Sc., B.Sc. : Physics.

## **Dr. Dibya Prakash Rai**

Post Doctoral Fellow (PDF), M.Sc., B.Sc., Working as Assistant Professor in Department of Physics in Pachhungga University College, Mizoram, India.

## **Dr. Pankaj Kumar Pal**

Ph.D R/S, ECE Deptt., IIT-Roorkee.

## **Dr. P. Thangam**

PhD in Information & Communication Engineering, ME (CSE), BE (Computer Hardware & Software), currently serving as Associate Professor in the Department of Computer Science and Engineering of Coimbatore Institute of Engineering and Technology.

## **Dr. Pradeep K. Sharma**

PhD., M.Phil, M.Sc, B.Sc, in Physics, MBA in System Management, Presently working as Provost and Associate Professor & Head of Department for Physics in University of Engineering & Management, Jaipur.

## **Dr. R. Devi Priya**

Ph.D (CSE), Anna University Chennai in 2013, M.E, B.E (CSE) from Kongu Engineering College, currently working in the Department of Computer Science and Engineering in Kongu Engineering College, Tamil Nadu, India.

## **Dr. Sandeep**

Post-doctoral fellow, Principal Investigator, Young Scientist Scheme Project (DST-SERB), Department of Physics, Mizoram University, Aizawl Mizoram, India- 796001.

## **Dr. Roberto Volpe**

Faculty of Engineering and Architecture, Università degli Studi di Enna "Kore", Cittadella Universitaria, 94100 – Enna (IT).

## **Dr. S. Kannadhasan**

Ph.D (Smart Antennas), M.E (Communication Systems), M.B.A (Human Resources).

**Research Area:** Engineering Physics, Electromagnetic Field Theory, Electronic Material and Processes, Wireless Communications.

## **Mr. Amit Kumar**

Amit Kumar is associated as a Researcher with the Department of Computer Science, College of Information Science and Technology, Nanjing Forestry University, Nanjing, China since 2009. He is working as a State Representative (HP), Spoken Tutorial Project, IIT Bombay promoting and integrating ICT in Literacy through Free and Open Source Software under National Mission on Education through ICT (NMEICT) of MHRD, Govt. of India; in the state of Himachal Pradesh, India.

## **Mr. Tanvir Singh**

Tanvir Singh is acting as Outreach Officer (Punjab and J&K) for MHRD Govt. of India Project: Spoken Tutorial - IIT Bombay fostering IT Literacy through Open Source Technology under National Mission on Education through ICT (NMEICT). He is also acting as Research Associate since 2010 with Nanjing Forestry University, Nanjing, Jiangsu, China in the field of Social and Environmental Sustainability.

## **Mr. Abilash**

M.Tech in VLSI, BTech in Electronics & Telecommunication engineering through A.M.I.E.T.E from Central Electronics Engineering Research Institute (C.E.E.R.I) Pilani, Industrial Electronics from ATI-EPI Hyderabad, IEEE course in Mechatronics, CSHAM from Birla Institute Of Professional Studies.

## **Mr. Varun Shukla**

M.Tech in ECE from RGPV (Awarded with silver Medal By President of India), Assistant Professor, Dept. of ECE, PSIT, Kanpur.

## **Mr. Shrikant Harle**

Presently working as a Assistant Professor in Civil Engineering field of Prof. Ram Meghe College of Engineering and Management, Amravati. He was Senior Design Engineer (Larsen & Toubro Limited, India).

## **Zairi Ismael Rizman**

Senior Lecturer, Faculty of Electrical Engineering, Universiti Teknologi MARA (UiTM) (Terengganu) Malaysia Master (Science) in Microelectronics (2005), Universiti Kebangsaan Malaysia (UKM), Malaysia. Bachelor (Hons.) and Diploma in Electrical Engineering (Communication) (2002), UiTM Shah Alam, Malaysia.

## **Mr. Ronak**

**Qualification:** M.Tech. in Mechanical Engineering (CAD/CAM), B.E.





Presently working as a Assistant Professor in Mechanical Engineering in ITM Vocational University, Vadodara. Mr. Ronak also worked as Design Engineer at Finstern Engineering Private Limited, Makarpura, Vadodara.



# Table of Contents

Volume-9, Issue-10, October 2023

S. No	Title	Page No.
1	<p><b>Equilibrium, Thermodynamics, Kinetics of Adsorption of CO<sub>3</sub><sup>2-</sup> and SO<sub>4</sub><sup>2-</sup> Ions on Modified Plantain Peels</b></p> <p><b>Authors:</b> Oyewole Toyib Seun, Inuikim Edak Asuquo, Osundiya Medinat Olubunmi, Osifeko Olawale Lawrence, Olowu Rasaq Adewale, Isaac Ibidun Blessing, Taiwo Rahman Olaseni, Adejare Adeniyi Ayemu, Oresanya Zechariah Oluwapelumi</p> <p> <b>DOI:</b> <a href="https://dx.doi.org/10.5281/zenodo.10053927">https://dx.doi.org/10.5281/zenodo.10053927</a></p> <p> <b>DIN Digital Identification Number:</b> IJOER-OCT-2023-1</p>	01-12
2	<p><b>Research into the Possibility of Regenerating Silica Gel using Vacuum</b></p> <p><b>Authors:</b> Romana Dobáková, Lukáš Tóth</p> <p> <b>DOI:</b> <a href="https://dx.doi.org/10.5281/zenodo.10053972">https://dx.doi.org/10.5281/zenodo.10053972</a></p> <p> <b>DIN Digital Identification Number:</b> IJOER-OCT-2023-2</p>	13-17
3	<p><b>Structural Design of Atypical Metal hydride Tank and Investigation of Generated Temperature Fields: Part I</b></p> <p><b>Authors:</b> Filip Duda, Natália Jasminská</p> <p> <b>DOI:</b> <a href="https://dx.doi.org/10.5281/zenodo.10054017">https://dx.doi.org/10.5281/zenodo.10054017</a></p> <p> <b>DIN Digital Identification Number:</b> IJOER-OCT-2023-3</p>	18-22
4	<p><b>Gas Transmission System Optimization with Natural Gas Transportation</b></p> <p><b>Authors:</b> Ľubomíra Kmeťová</p> <p> <b>DOI:</b> <a href="https://dx.doi.org/10.5281/zenodo.10054037">https://dx.doi.org/10.5281/zenodo.10054037</a></p> <p> <b>DIN Digital Identification Number:</b> IJOER-OCT-2023-4</p>	23-28
5	<p><b>Design of A Model of Liquid Feeder to an Incinerator of Hazardous Waste and its Optimization from the Cooling Point of View: Part I</b></p> <p><b>Authors:</b> Ivan Mihálik, Marián Lázár, Tomáš Brestovič</p> <p> <b>DOI:</b> <a href="https://dx.doi.org/10.5281/zenodo.10054221">https://dx.doi.org/10.5281/zenodo.10054221</a></p> <p> <b>DIN Digital Identification Number:</b> IJOER-OCT-2023-5</p>	29-34

6	<p><b>Design of An Experimental Device for the Analysis of the Influence of Sound Waves on the CPU Cooling Process - Part I</b></p> <p><b>Authors:</b> Lukáš Tóth, Romana Dobáková</p> <p> <b>DOI:</b> <a href="https://dx.doi.org/10.5281/zenodo.10054234">https://dx.doi.org/10.5281/zenodo.10054234</a></p> <p> <b>DIN Digital Identification Number:</b> IJOER-OCT-2023-6</p>	35-40
7	<p><b>Device for Researching the Cooling Intensity of Flowing Media</b></p> <p><b>Authors:</b> Mária Čarnogurská, Miroslav Příhoda, Tomáš Brestovič</p> <p> <b>DOI:</b> <a href="https://dx.doi.org/10.5281/zenodo.10054242">https://dx.doi.org/10.5281/zenodo.10054242</a></p> <p> <b>DIN Digital Identification Number:</b> IJOER-OCT-2023-7</p>	41-45

# Equilibrium, Thermodynamics, Kinetics of Adsorption of $\text{CO}_3^{2-}$ and $\text{SO}_4^{2-}$ Ions on Modified Plantain Peels

Oyewole Toyib Seun<sup>1\*</sup>, Inuikim Edak Asuquo<sup>2</sup>, Osundiya Medinat Olubunmi<sup>3</sup>,  
Osifeko Olawale Lawrence<sup>4</sup>, Olowu Rasaq Adewale<sup>5</sup>, Isaac Ibidun Blessing<sup>6</sup>,  
Taiwo Rahman Olaseni<sup>7</sup>, Adejare Adeniyi Ayemu<sup>8</sup>, Oresanya Zechariah Oluwapelumi<sup>9</sup>

<sup>1-5, 7-9</sup>Department of Chemistry, Lagos State University, Ojo, Nigeria

<sup>6</sup>Department of Chemistry, University of Missouri, Saint Louis, USA

\*Corresponding Author

Received: 04 October 2023/ Revised: 16 October 2023/ Accepted: 21 October 2023/ Published: 31-10-2023

Copyright © 2023 International Journal of Engineering Research and Science

This is an Open-Access article distributed under the terms of the Creative Commons Attribution

Non-Commercial License (<https://creativecommons.org/licenses/by-nc/4.0>) which permits unrestricted

Non-commercial use, distribution, and reproduction in any medium, provided the original work is properly cited.

**Abstract**— To reuse treated wastewater, water quality must be improved. Adsorption is a simple, cost-effective method for eliminating toxicities and poisonous anions. The adsorbent's features and properties determine the method's effectiveness. This research examines the adsorption of carbonate and sulphate anions onto plantain peels modified with 2-amino-4,6-dihydropyrimidine. Characterization was done using SEM, XRD, and FTIR. UV-visible spectroscopy was used to measure initial and equilibrium concentrations, and Langmuir and Freundlich isotherms were used to analyze the data. The best parameters for adsorbing 150 mg/L  $\text{CO}_3^{2-}$  and  $\text{SO}_4^{2-}$  were: pH 2, and 4, 0.8 g adsorbent, 120 min contact time, and 330 K temperature. Kinetic study used pseudo-first-order reaction equations, and both ion uptake processes followed pseudo-first-order rate expression.  $\Delta G$  (-3.772 kJ/mol) for  $\text{CO}_3^{2-}$  and  $\Delta G$  (-3.047 kJ/mol) for  $\text{SO}_4^{2-}$  were negative, and  $\Delta H$  (-22.04 kJ/mol) and (-39.92 kJ/mol) were also negative, indicating the adsorption process was feasible, spontaneous, and exothermic. Modified plantain peels had high adsorptivity and were a cost-effective adsorbent for  $\text{CO}_3^{2-}$  and  $\text{SO}_4^{2-}$  from aqueous solutions.

**Keywords**— 2-amino-4,6-dihydropyrimidine, Anions, Isotherm, Plantain peels, Thermodynamic.

## I. INTRODUCTION

Toxic anions polluting groundwater is a global problem endangering drinking water. Excessive use and discharge of phosphorus, nitrogen, and sulphur compounds raise nutrient levels in surface and groundwater. When toxic metals enter the environment, metal ions accumulate in humans through direct ingestion or food chains. Water is a fundamental resource for humanity, and its protection is essential for present and future societies. Human activities, like industrial practices, domestic waters, and agricultural uses (e.g. fertilizers, compost, wastewater treatment effluent) often contaminate water with nitrate, sulphate, and phosphate[1]. Recent technological and economic developments are creating toxic pollutants in the different sources of natural water and this is constituting a major hazard to human health [3]. With over 1.2 billion people lacking access to clean, unpolluted, and safe drinking water, water-related issues especially as regards the ever-increasing water scarcity and water pollution remains one of the most topical issues of environmental [2]. Higher levels of sulfate in drinking water lead to its bitter taste and digestive problems as well as corrosion of sewer pipes in addition to causing problems in the anaerobic wastewater treatment processes [4].

Improving water quality is essential for wastewater reuse. Health risks must be taken into account, which could lead to stricter water quality standards [5]. Common mercury removal techniques include adsorption [6], ion exchange, flocculation, and ultrafiltration. Adsorption is a simple, adaptable, and established technique for removing heavy metals, including mercury, from industrial wastewater [7]. It is cost-effective and does not require advanced technology. Deep filtration, macro-filtration, and adsorption can remove some toxic anions, while disinfection eliminates the rest [7].

Wastewater purification using adsorption is a simple, economical way to remove toxins and metals. The adsorbent's features and properties determine the method's effectiveness. Adsorption isotherm is the fundamental concept in adsorption. Equilibrium between pressure/concentration in the bulk fluid phase and adsorbed quantity is known as adsorption. Banana peel and its modified forms are cost-effective and widely available, making them popular adsorbents for wastewater treatment (5-

6). Cellulosic agricultural waste, such as banana peel, is abundant, cheap, and can remove heavy metals from wastewater. It has been demonstrated to have a high capacity for heavy metal removal[9].

Several studies have explored the adsorption of heavy metals onto solid surfaces for separation and pre-concentration of complex mixtures, single elements, and series [10]. Reverse osmosis and filtration are expensive for developing countries like Nigeria, so low-cost adsorbent materials are needed to remove anions and heavy metals globally [11].

Thus, this research is, therefore, an inclusive part of the ongoing process of developing an alternative technology for utilizing cheap plantain peels modified with 2-amino-4,6-dihydroxypyrimidine (ligand) to study the kinetics, equilibrium, and thermodynamics of adsorption of carbonate ( $\text{CO}_3^{2-}$ ) and sulphate ( $\text{SO}_4^{2-}$ ) anion on modified plantain peels.

## II. MATERIALS AND METHODS

2-amino-4,6-dihydroxypyrimidine (ligand) was obtained from Sigma Aldrich, India. All other reagents were of analytical grade. Plantain peels were bought from a local market in Ajah, Lagos Island, Nigeria. Deionized water was used throughout.

### 2.1 Preparation of Modified Biosorbent

1.5 g of the ligand was dissolved in 1000ml sodium hydroxide and stirred until colorless. Samples of 5 g, 10 g, and 25 g were weighed and mixed with 50ml, 70ml, and 100ml of ligand respectively. The mixtures were shaken for 70 hours to ensure the ligand was well adsorbed by the plantain peels. The reaction process is as follows:

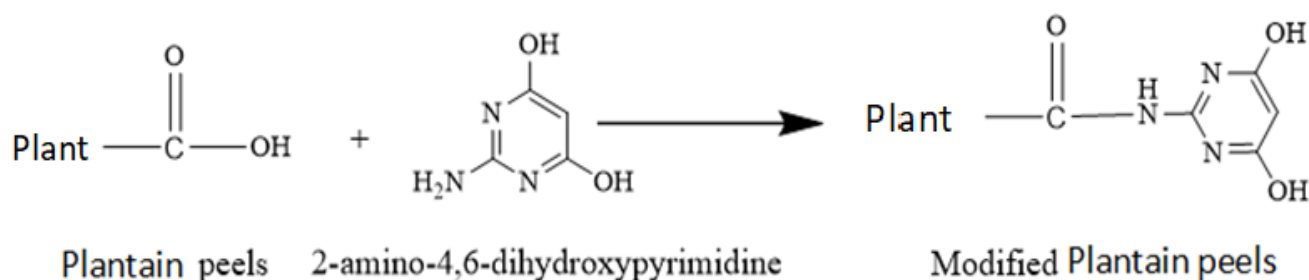


FIGURE 1: Reaction between plantain peel and the ligand

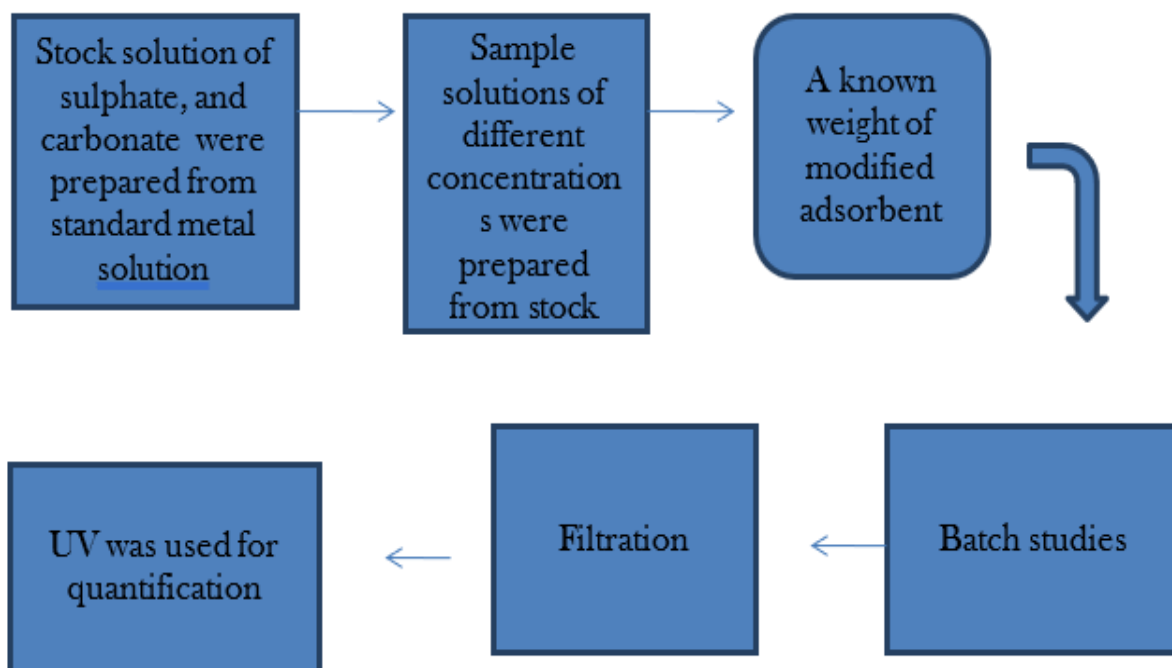


FIGURE 2: Organogram for sample preparation and quantification



**FIGURE 3: (a, b, c, and d): Dried plantain peels, pulverized plantain peel, modified plantain peel on shaker, and dried modified plantain peel respectively.**

## 2.2 Adsorption Kinetics

Adsorption kinetics offers insights into the adsorbent's service time, adsorption mechanisms, and adsorption-adsorbent interactions. However, choosing appropriate models for sorption data analysis is challenging due to the plethora of kinetic models. The adsorption kinetic was studied at 25 °C using 0.2 g in 100 mL solution at 100 mg/L, sampled at intervals until 150 min. UV-Vis spectrophotometry at 800 nm and 420 nm determined the final carbonate and sulphate concentrations. Equation (1) calculated the adsorption capacity.

$$q_t = \frac{C_i - C_f}{m} \times V \quad (1)$$

Where  $q_t$  is the adsorption capacity at time  $t$ ,  $C_i$  and  $C_f$  are the initial and equilibrium concentration respectively, in mg/L,  $V$  is the volume of the solution and  $m$  is the mass of the adsorbent in g

The kinetics of adsorption can be described by different models, some of which include:

Pseudo-first order Lagrange model considers the rate of change that occurs in the uptake of adsorbate at a particular reaction time to be directly proportional to the difference in the concentration and rate at which the adsorbate is removed with time. The model is represented by the equation below:

$$\frac{dq_t}{dt} = K_t (q_e - q_t) \quad (2)$$

The integral form is given as;

$$\text{Log} (q_e - q_t) = \text{Log} (q_e) - \left(\frac{K_t}{2.303}\right)t \quad (3)$$

Where  $q_e$  (mg/g) is the adsorption capacity of the adsorbent at equilibrium.

$Q_t$  (mg/g) is the adsorption capacity of the adsorbent at time,  $t$ .

$K_t$  (per min) is the rate constant for pseudo-first-order adsorption.

The plot of  $\text{Log} (q_e - q_t)$  versus  $t$  gives a relationship that is linear from which  $K_t$  and  $q_e$  can be determined from the slope and intercept of the plot.

Pseudo-second-order kinetics: The pseudo-second-order model proposes that the rate of adsorption is proportional to the square of the concentration of the adsorbate on the surface. This model takes into account the possibility of a two-step adsorption process, involving chemisorption or strong physical adsorption [13]. It provides a better fit for adsorption processes where the initial concentration is closer to the equilibrium concentration. The model assumes that one metal ion is adsorbed onto two sorption sites on the adsorbate surface. The PSEUDO-SECOND ORDER linear expression is given as:

$$\frac{t}{q} = \frac{1}{K_2 q_e^2} + \frac{1}{q_e} t \quad (4)$$

## 2.3 Adsorption Isotherm

Freundlich and Langmuir models are two of the most popular adsorption isotherm models for activated carbon in water and wastewater treatment [14]. They describe the relationship between adsorbate concentration and adsorbent loading. This research studied adsorption isotherm models. Adsorption is a process where adsorbate and adsorbent come into contact and

equilibrium isotherm is established when the adsorbate concentration in the solution is balanced with the interface concentration [15]. The Langmuir isotherm, for monomolecular adsorption, is:

$$q_e = \frac{q_m K_L C_e}{1 + K_L C_e} \quad (5)$$

The linearized form of the equation is given as:

$$\frac{C_e}{q_e} = \frac{1}{q_m K_L} + \frac{C_e}{q_m} \quad (6)$$

Where  $C_e$  is the equilibrium metal concentration,  $K_L$  and  $q_m$  are the Langmuir constants related to maximum adsorption capacity (mg/g), and the relative energy of adsorption (1/mg) respectively.

The Freundlich Isotherm Model is another approach that is used for the description of the multilayer and heterogeneous adsorption of molecules to the adsorbent surface. This model is demonstrated by the equation:

$$\ln q_e = \ln K_f + \frac{1}{n} \ln C_e \quad (7)$$

Where  $q_m$  (mg/g) represents the amount of adsorbed molecules to the adsorbent surface at any time,  $C_e$  (mg/L) is the equilibrium concentration,  $K_f$  (mg/g) indicates the adsorption capacity of the adsorbent towards the adsorbate and  $n$  is an indicator for the degree of homogeneity and describes the distribution of the adsorbed molecules on the adsorbent surface. A value of  $n$  higher than 1, indicates a favorable adsorption of the molecules onto the adsorbent surface. A value of higher  $n$  reflects the higher intensity of adsorption.

## 2.4 Thermodynamic studies

Thermodynamic parameters are very important for adsorption studies, indicating the spontaneity of the adsorption process [17]. The negative value of Gibb's free energy change ( $\Delta G^\circ$ ) for a given temperature indicates the spontaneity of the adsorption process [18]. Among the parameters, Gibb's free energy change ( $\Delta G^\circ$ ) was calculated using Equation (8):

$$\Delta G^\circ = -RT \ln K_a \quad (8)$$

While the change in enthalpy ( $\Delta H^\circ$ ) and change in entropy ( $\Delta S^\circ$ ) were determined using the Equation,

$$\ln K_a = \frac{\Delta S^\circ}{R} - \frac{\Delta H^\circ}{RT} \quad (9)$$

Where  $R$  is the gas constant (8.314 J/mol K),  $T$  is the temperature in Kelvin (K) and,  $K_a$  is the Langmuir constant.

## III. RESULTS AND DISCUSSIONS

### 3.1 Fourier Transform Infrared Spectroscopy (FTIR)

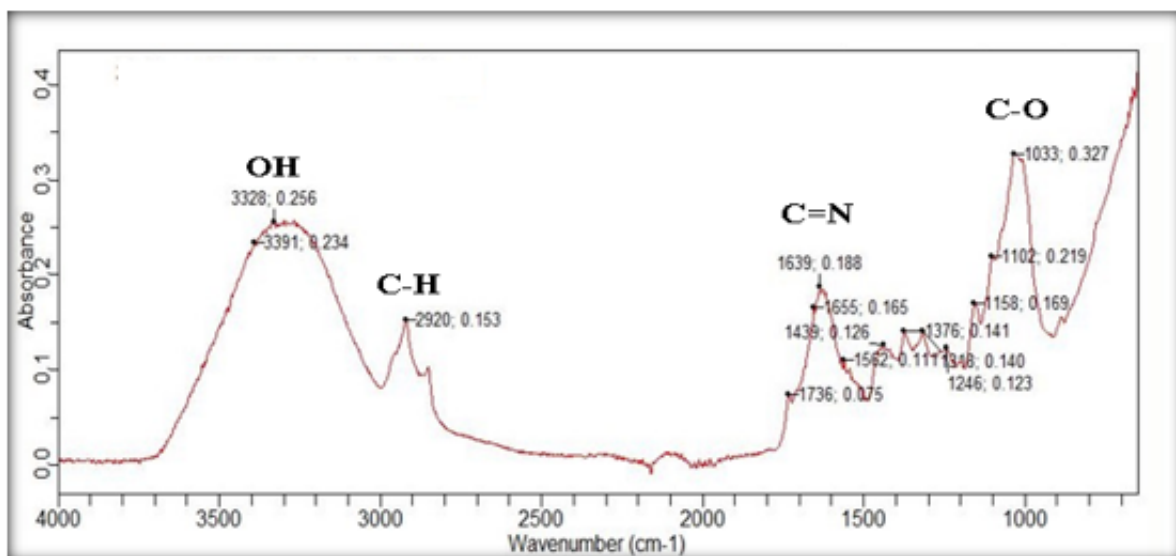


FIGURE 4: FTIR image for modified plantain peel.

FTIR spectrum of modified plantain peel was recorded to identify functional groups coordinating with ions. Figure 4 shows the FTIR spectrum of 1.30 mm size mesh dried plantain peels. The broad band at  $3328\text{ cm}^{-1}$  indicates O-H stretching of carboxylic acid. The  $2920\text{ cm}^{-1}$  band indicates C-H stretching of alkane,  $1639\text{ cm}^{-1}$  is C=N imine stretching, and  $1033\text{ cm}^{-1}$  is C-O stretching of primary alcohol. The  $1639\text{ cm}^{-1}$  peak confirms ligand presence, indicating modification of plantain peels.

### 3.2 Scanning Electron Microscope (SEM)

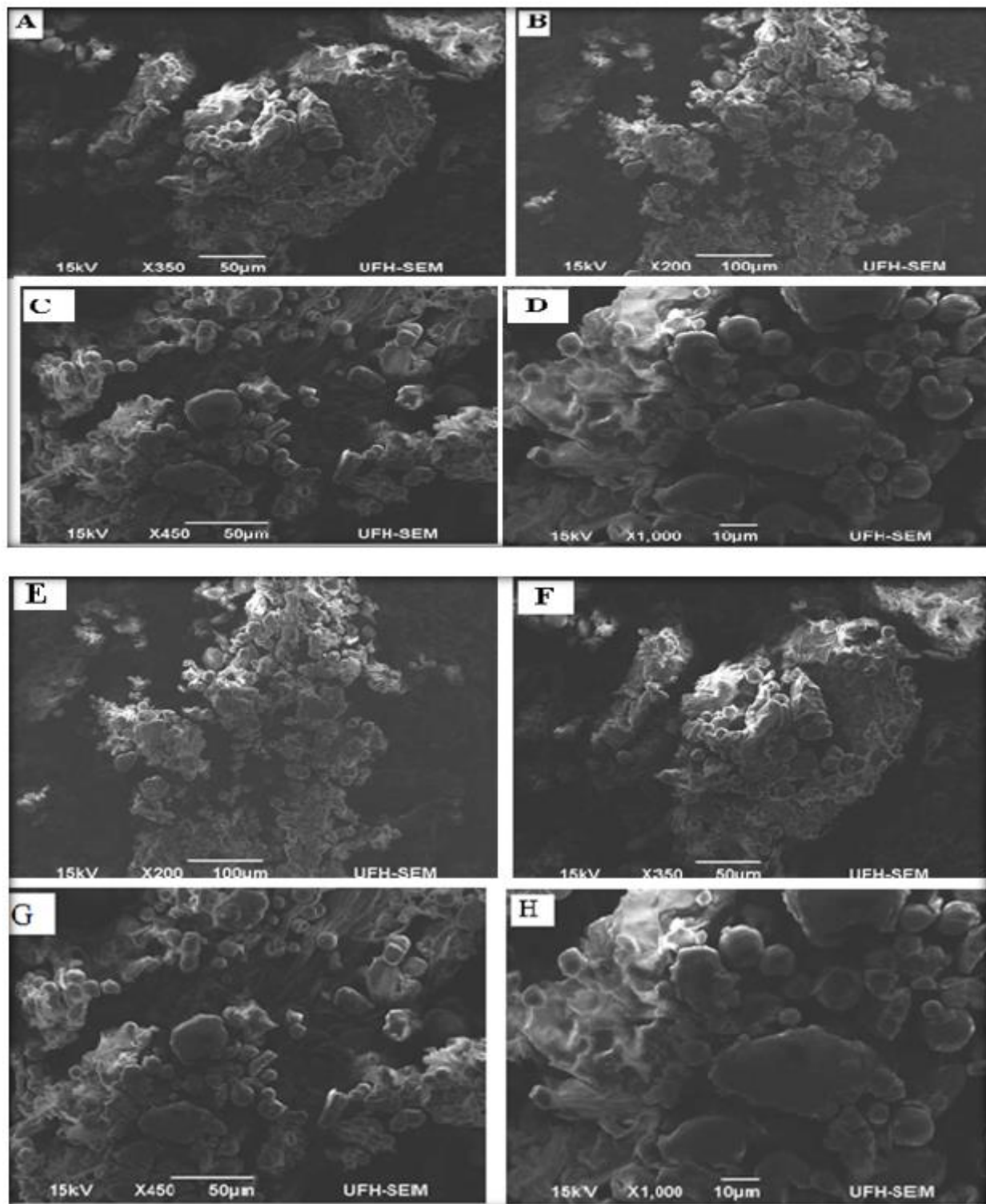


FIGURE 5: (A-D and E-H): SEM images of sieved and unsieved plantain peels before adsorption (A-D and E-H, respectively)

The Scanning electron microscope (SEM) was used to analyze the adsorbate's surface morphology before and after adsorption. Figure 5 displays the results with a different scale bar. SEM also showed the toxic anions adsorbed onto the modified plantain peels. The results showed the adsorbent material's surface morphology, which affects adsorption capacity and efficiency due to features like pore size, cracks, and roughness.

### 3.3 X-ray Diffraction (XRD)

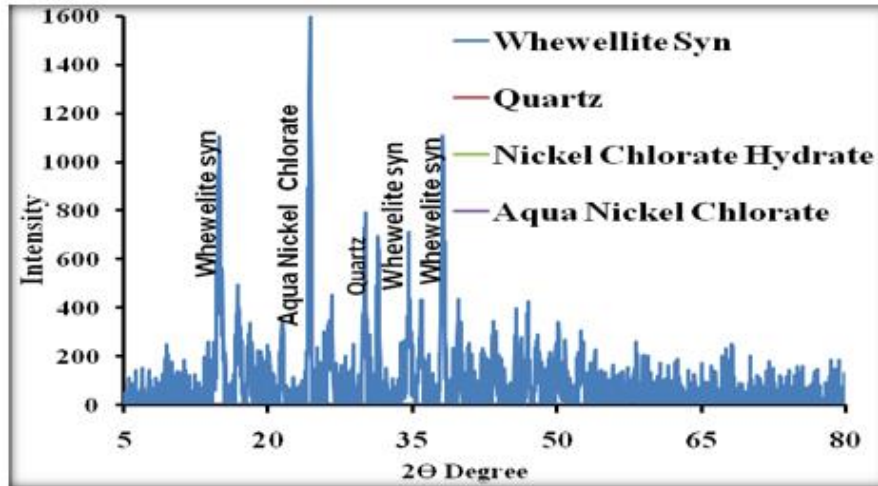


FIGURE 6: XRD image For Pulverized Sieved Plantain Peels

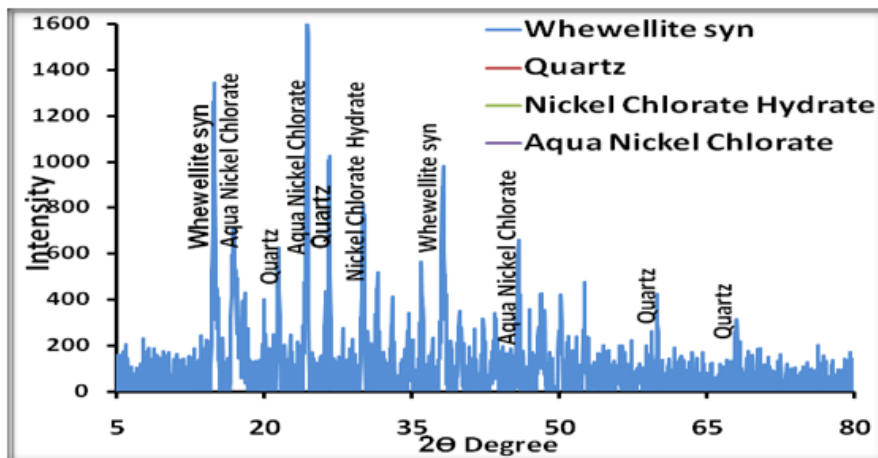


FIGURE 7: Shows XRD For Pulverized Unsieved Plantain Peels

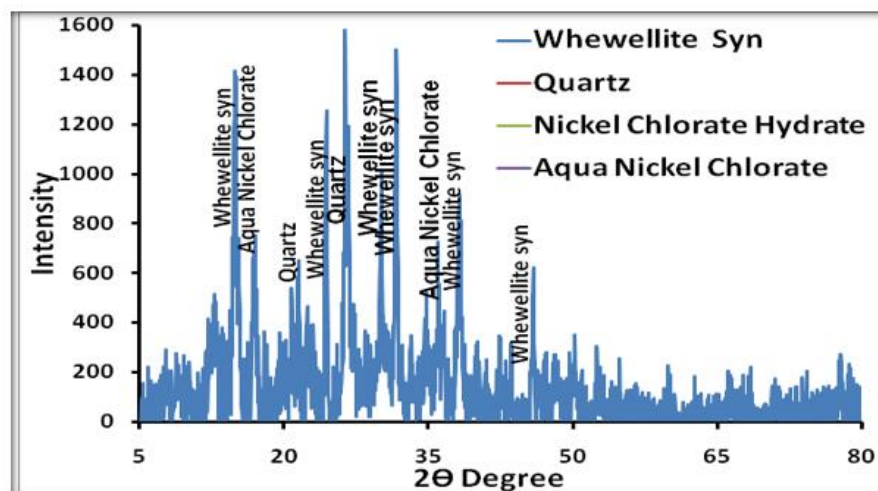


FIGURE 8: Shows XRD For Pulverized Sieved Residue Plantain Peels



The XRD graph displays the minerals in pulverized sieved, unsieved, and sieved residue. The main minerals are whewellite, quartz, aqua nickel chlorate, and nickel chlorate hydrate (Table 1). The pulverized sieved (Figure 7) and sieved residue (Figure 8) have the highest peak of 1600 with aqua nickel hydrate, while the unsieved (Figure 8) has quartz with the highest peak. The most common peak in the three samples was whewellite syn.

**TABLE 1**  
**XRD MINERAL PHASES IN PULVERIZED SIEVED, UNSIEVED, AND SIEVED RESIDUE PLANTAIN PEEL**

Mineral Phase	Formula	Number
WhewelliteSyn	$C_2CaO_4.H_2O / CaO_4.H_2O$	00 – 020 – 0231
Quartz	$SiO_2$	01 – 083 – 0539
Nickel chlorate hydrate	$Ni(ClO_3)_2.6H_2O$	00 – 016 – 0195
Aqua nickel chlorate	$(Ni(H_2O)_6(ClO_3))$	01 – 079 – 1895

### 3.4 Adsorption Equilibrium Studies:

#### 3.4.1 Equilibrium Studies on the Effect of Contact Time:

The adsorbent capacity was studied considering the contact time of the solution at the solid/liquid interface. Contact time is an important factor in batch adsorption. Figure 10 shows that the removal efficiency of carbonate and sulphate ions onto the functionalized plantain peel adsorbent increases rapidly in the initial adsorption stage (30-150 min), then slowly until equilibrium is reached after 120 min.

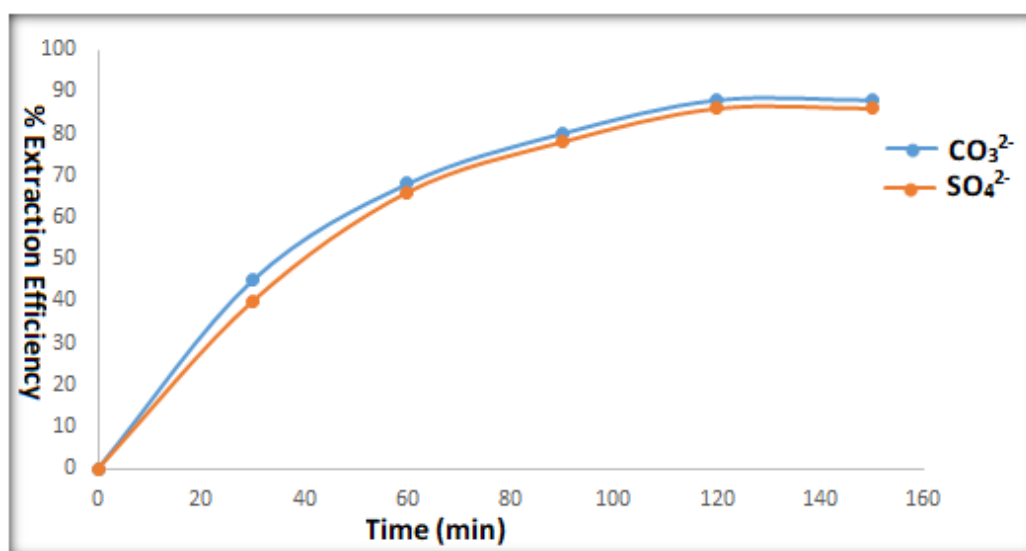


**FIGURE 9: Effect of contact time on carbonate and sulfate removal unto functionalized plantain peel**

#### 3.4.2 Equilibrium Studies on the Effect of pH

The impact of pH on adsorbate removal ( $CO_3^{2-}$  and  $SO_4^{2-}$ ) by modified plantain peel was studied, as shown in Figure 11. The highest capacities occurred between pH 2 and 4. In acidic conditions,  $H^+$  in the solution increased, making the sorbent surface positively charged, facilitating adsorption of negative anions [19]. The maximum removal of  $CO_3^{2-}$  and  $SO_4^{2-}$  was 89% and 83% respectively, possibly due to the electrostatic attraction between the acidic proton and the anions.

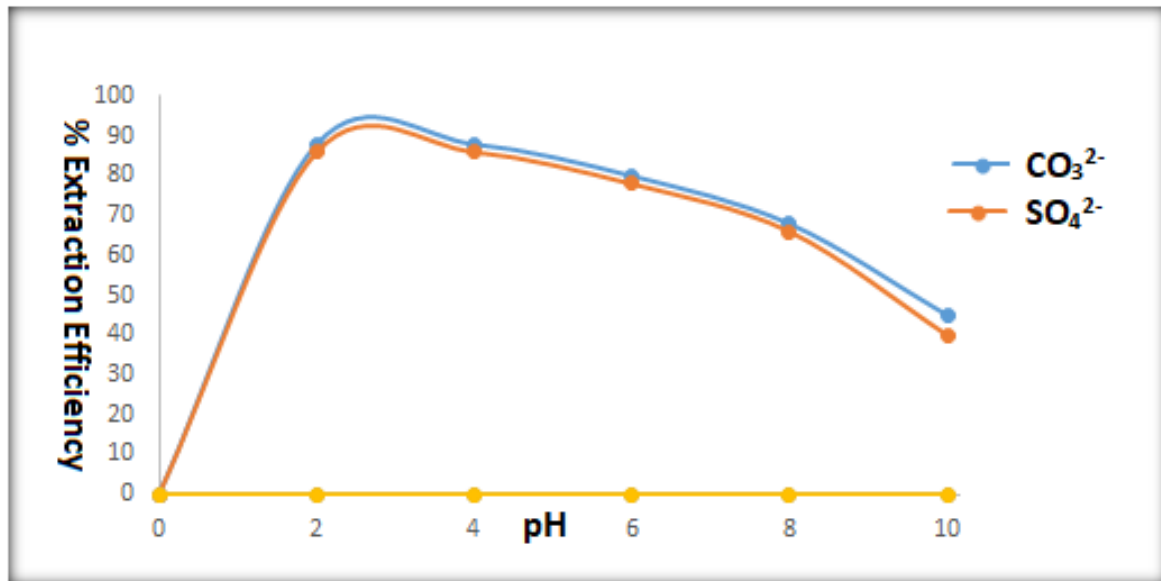


FIGURE 10: Effect of pH of carbonate and sulfate removal unto functionalized plantain peel.

### 3.4.3 Equilibrium Studies on the Effect of Concentration

Carbonate and sulphate concentrations effect on adsorption rate was studied at pH 4, 29 °C, and 120 min contact time in the range (50-250 mg/L). Figure 12 showed that 150 mg/L had the highest adsorbate removal, reaching equilibrium. The low concentration ratio of initial CO<sub>3</sub><sup>2-</sup> and SO<sub>4</sub><sup>2-</sup> ions to fixed sites caused more substances to occupy the interlayer space, reducing ion removal. The highest CO<sub>3</sub><sup>2-</sup> and SO<sub>4</sub><sup>2-</sup> removal was 90% and 68% with functionalized plantain peel, respectively.

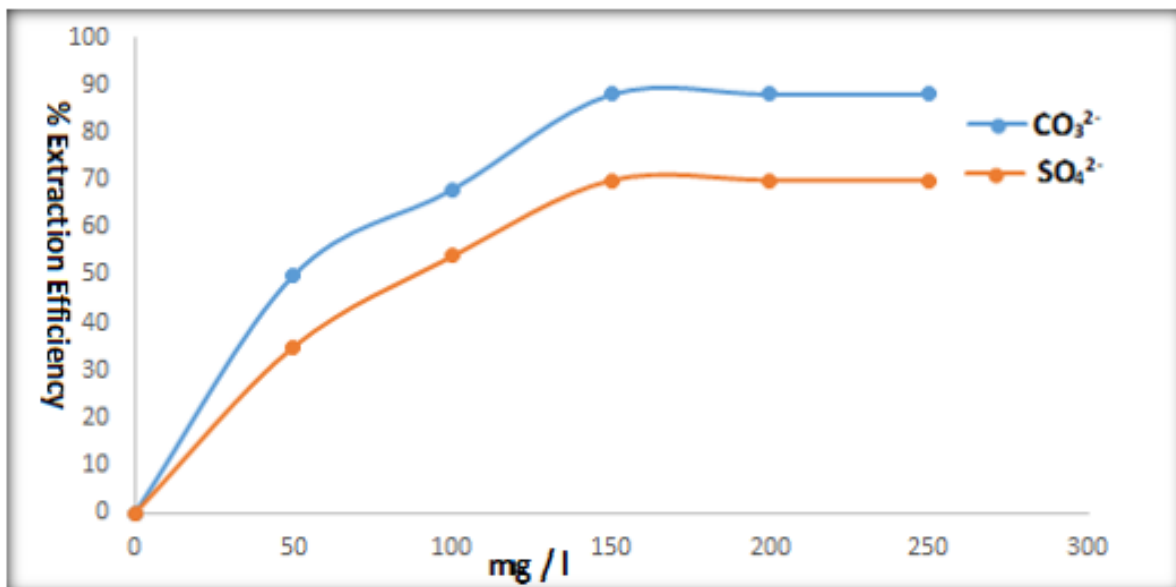
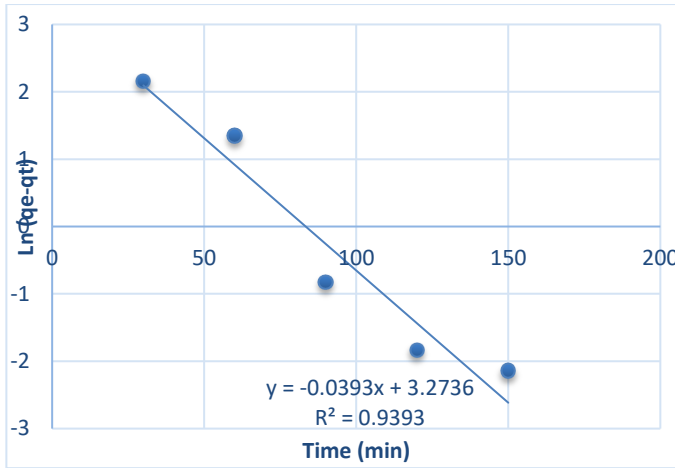


FIGURE 11: The effect of the concentration of carbonate and sulfate removal on unfunctionalized plantain peel

### 3.5 Adsorption Kinetic Studies

The adsorption kinetics of the adsorption experiments were determined by the pseudo-first-order reaction. The contact time ranges from 30-150 min. the result in Figures 13, and 14 indicate that the experimental data for this study was fitted for a pseudo-first-order kinetic model due to the R<sup>2</sup> value that is closer to the unity.



**FIGURE 12: Pseudo-first-order kinetics plot for  $\text{CO}_3^{2-}$**

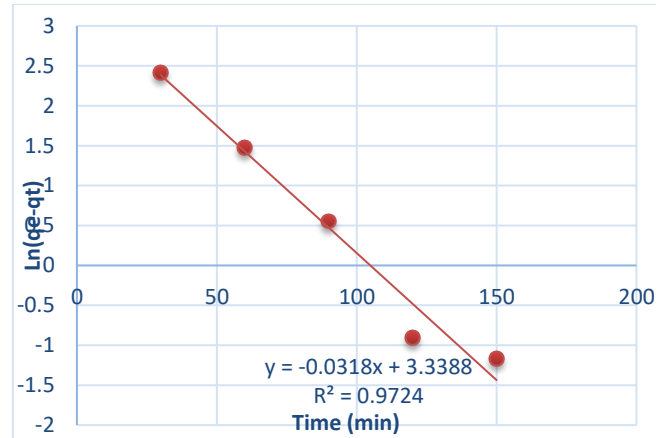


**FIGURE 13: Pseudo first-order kinetics plot for  $\text{SO}_4^{2-}$**

**3.6 Adsorption Isotherm Studies**

Equilibrium data for adsorption are generally known as adsorption isotherms. In this research, two (2) isotherm models were used: the Langmuir and Frenunlich isotherms applying equations (8) and (10) respectively. Various constants of the models are also calculated and shown in table 2 and 3.

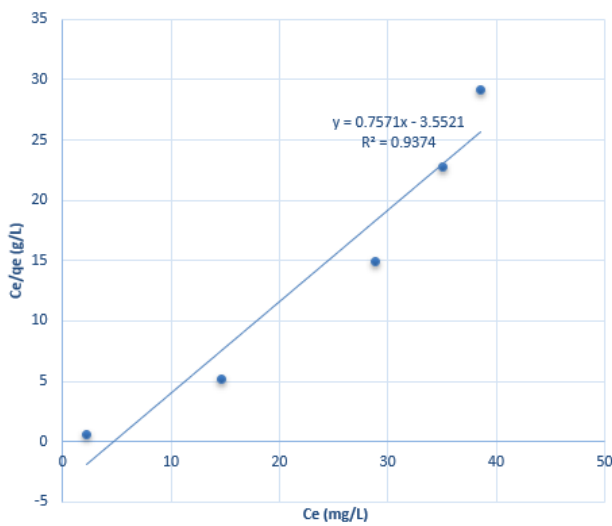


**FIGURE 14: Langmuir adsorption isotherm for  $\text{CO}_3^{2-}$**

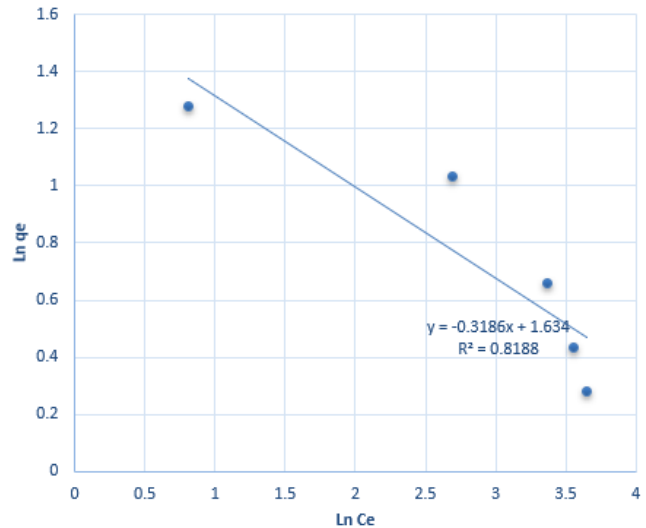


**FIGURE 15: Freundlich adsorption isotherm for  $\text{CO}_3^{2-}$**

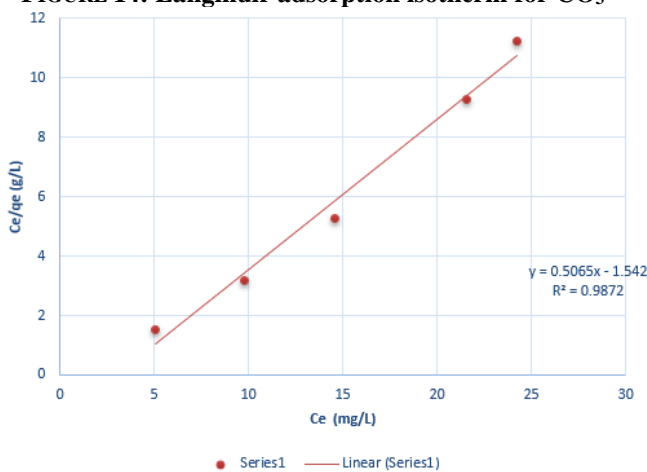


**FIGURE 16: Langmuir adsorption isotherm for  $\text{SO}_4^{2-}$**

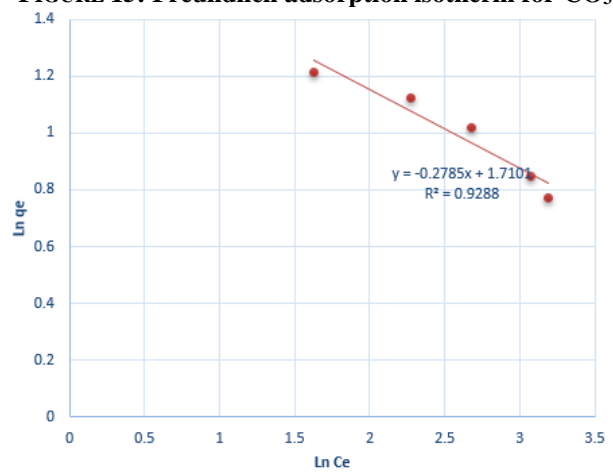


**FIGURE 17: Freundlich adsorption isotherm for  $\text{SO}_4^{2-}$**

**TABLE 2**  
**ISOTHERM CONSTANTS FOR CO<sub>3</sub><sup>2-</sup> ADSORPTION**

Langmuir	Values	Freundlich	Values
Q <sub>m</sub> (mg/L)	1.867	K <sub>f</sub> (mg/Kg)	4.231
K <sub>1</sub> (L/mg)	0.311	N	0.145
R <sup>2</sup>	0.987	R <sup>2</sup>	0.928
R <sub>1</sub>	0.06		

**TABLE 3**  
**ISOTHERM CONSTANTS FOR SO<sub>4</sub><sup>2-</sup> ADSORPTION**

Langmuir	Values	Freundlich	Values
Q <sub>m</sub> (mg/L)	1.662	K <sub>f</sub> (mg/Kg)	3.426
K <sub>1</sub> (L/mg)	0.421	N	0.115
R <sup>2</sup>	0.937	R <sup>2</sup>	0.818
R <sub>1</sub>	0.05		

**3.7 Thermodynamic Parameters**

The results of the various thermodynamic parameters for the adsorption of CO<sub>3</sub><sup>2-</sup> and SO<sub>4</sub><sup>2-</sup> ions are shown in Table 4 and 5 below:

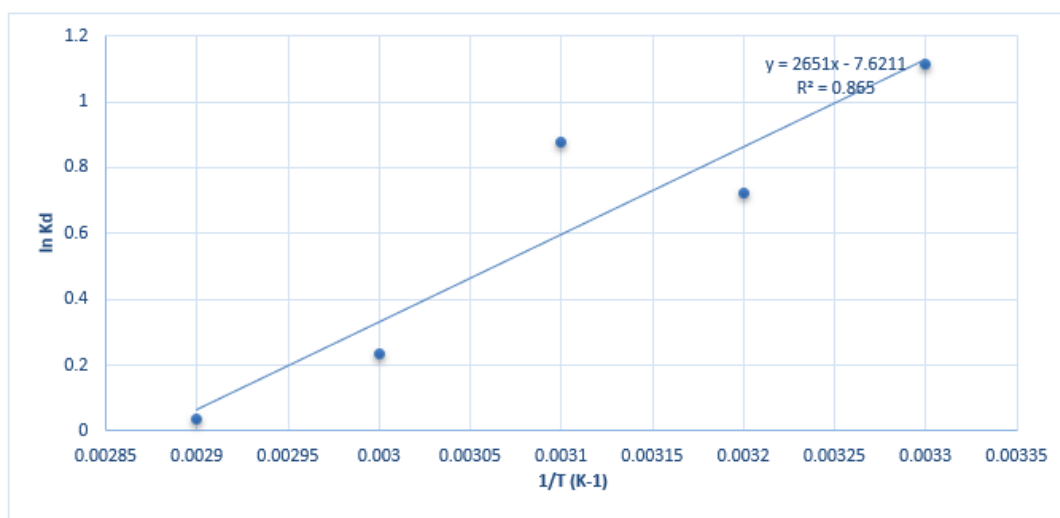


**FIGURE 18: Thermodynamics plot for CO<sub>3</sub><sup>2-</sup>**

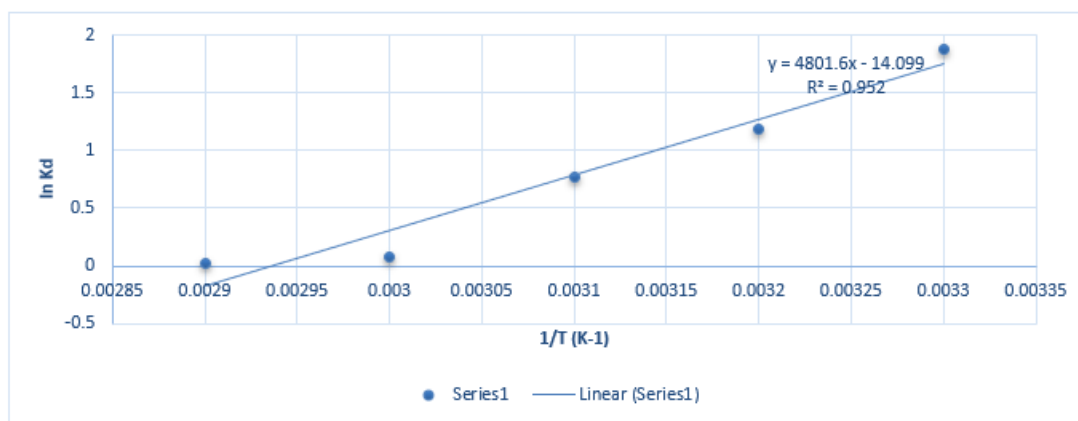


**FIGURE 19: Thermodynamics plot for SO<sub>4</sub><sup>2-</sup>**

**TABLE 4**  
**THERMODYNAMIC PARAMETERS FOR CO<sub>3</sub><sup>2-</sup> ADSORPTION**

T(K)	LnK	ΔG (KJ/mol)	ΔH (KJ/mol)	ΔS (J/mol/K)
299	1.115	-2.772		
309	0.723	-1.857		
319	0.879	-2.331		
329	1.379	-3.772	-22.04	-63.362
339	0.900	-2.537		

**TABLE 5**  
**THERMODYNAMIC PARAMETERS FOR SO<sub>4</sub><sup>2-</sup> ADSORPTION**

T(K)	LnK	ΔG (KJ/mol)	ΔH (KJ/mol)	ΔS (J/mol/K)
299	1.875	-4.661		
309	1.186	-3.047	-39.92	-117.219
319	0.765	-2.029		
329	0.078	-0.213		
339	0.0282	-0.079		

#### IV. CONCLUSION

Research showed modified natural adsorbents can remove anion pollutants from water, with effectiveness depending on adsorbent dose, temperature, concentration, pH, and contact time. The pseudo-first-order kinetic model and Langmuir model fit the adsorption and equilibrium isotherm data well, respectively. RL values indicated modified plantain peels were suitable for anion adsorption. Thermodynamic analysis revealed the reaction was spontaneous, exothermic, and physisorption. Thus, modified plantain peels are a promising, low-cost adsorbent for carbonate and sulphate ion removal from aqueous solutions.

#### REFERENCES

- [1] E. Study, "Selective and Competitive Adsorption of Anions in Solution on Porous Adsorbent from Zea mays Steams: Kinetic and," 2022.
- [2] C. O. Thompson, A. O. Ndukwe, and C. O. Asadu, "Application of activated biomass waste as an adsorbent for the removal of lead (II) ion from wastewater," *Emerg. Contam.*, vol. 6, pp. 259–267, 2020, doi: 10.1016/j.emcon.2020.07.003.
- [3] P. Moens, F. Callens, P. Matthys, F. Maes, R. Verbeeck, and D. Naessens, "Adsorption of carbonate-derived molecules on the surface of carbonate-containing apatites," *J. Chem. Soc. Faraday Trans.*, vol. 87, no. 19, pp. 3137–3141, 1991, doi: 10.1039/FT9918703137.
- [4] A. Naghizadeh, F. Ghasemi, E. Derakhshani, and H. Shahabi, "Thermodynamic, kinetic and isotherm studies of sulfate removal from aqueous solutions by graphene and graphite nanoparticles," *Desalin. Water Treat.*, vol. 80, pp. 247–254, 2017, doi: 10.5004/dwt.2017.20891.
- [5] A. H. Lahuri, M. A. Yarmo, N. Nordin, N. Dzakaria, A. H. I. Ing, and S. J. S. Kuda, "Adsorption Isotherm and Surface Analysis for the Carbonate Formation on Nano Coral-Shaped Iron(III) Oxide," *Sains Malaysiana*, vol. 52, no. 1, pp. 129–138, 2023, doi: 10.17576/jsm-2023-5201-10.
- [6] A. Imessaoudene *et al.*, "Adsorption Performance of Zeolite for the Removal of Congo Red Dye: Factorial Design Experiments, Kinetic, and Equilibrium Studies," *Separations*, vol. 10, no. 1, 2023, doi: 10.3390/separations10010057.
- [7] M. S. I. Syafiqah and H. W. Yussof, "ScienceDirect Kinetics, Isotherms, And Thermodynamic Studies on the Adsorption of Mercury (II) Ion from Aqueous Solution Using Modified Palm Oil Fuel Ash," *Mater. Today Proc.*, vol. 5, no. 10, pp. 21690–21697, 2018, doi: 10.1016/j.matpr.2018.07.020.
- [8] P. S. M. Gawande, N. S. Belwalkar, and A. A. Mane, "Adsorption and its Isotherm – Theory," no. June, 2017, doi: 10.5958/2319-6890.2017.00026.5.
- [9] M. JM, S. GS, and de B. M, "Adsorption of Mn<sup>2+</sup> from the Acid Mine Drainage using Banana Peel," *Int. J. Water Wastewater Treat.*, vol. 4, no. 1, pp. 1–9, 2018, doi: 10.16966/2381-5299.153.
- [10] R. A. Olowu, "Equilibrium and Kinetic Studies for the Removal of Zn (II) and Cr (VI) Ions from Aqueous Solution Using Pineapple Peels as an Adsorbent," vol. 10, no. 5, 2022.
- [11] A. H. Lahuri, M. L. Nguang Khai, A. A. Rahim, and N. Nordin, "Adsorption kinetics for CO<sub>2</sub> capture using cerium oxide impregnated

- on activated carbon,” *Acta Chim. Slov.*, vol. 67, no. 2, pp. 570–580, 2020, doi: 10.17344/ACSI.2019.5572.
- [12] A. N. Ebelegi, N. Ayawei, and D. Wankasi, “Interpretation of Adsorption Thermodynamics and Kinetics,” no. August, 2020, doi: 10.4236/ojpc.2020.103010.
- [13] R. Ragadhita and A. B. D. Nandiyanto, “How to calculate adsorption isotherms of particles using two-parameter monolayer adsorption models and equations,” *Indones. J. Sci. Technol.*, vol. 6, no. 1, pp. 205–234, 2021, doi: 10.17509/ijost.v6i1.32354.
- [14] F. J. Ogbozige and M. A. Toko, “Iranian ( Iranica ) Journal of Energy & Environment Adsorption Isotherms and Kinetics of Lead and Cadmium Ions : Comparative Studies Using Modified Melon ( Citrullus colocynthis ) Husk,” vol. 11, no. 2, pp. 157–162, 2020.
- [15] Y. John, V. E. David, and D. Mmereki, “A Comparative Study on Removal of Hazardous Anions from Water by Adsorption: A Review,” *Int. J. Chem. Eng.*, vol. 2018, no. Iii, pp. 1–21, 2018, doi: 10.1155/2018/3975948.
- [16] A. M. Anshar, P. Taba, and I. Raya, “Kinetic and thermodynamics studies on the adsorption of phenol on activated carbon from rice husk activated by ZnCl<sub>2</sub>,” *Indones. J. Sci. Technol.*, vol. 1, no. 1, pp. 47–60, 2016, doi: 10.17509/ijost.v1i1.2213.
- [17] D. Cordell and S. White, “Peak phosphorus: Clarifying the key issues of a vigorous debate about long-term phosphorus security,” *Sustainability*, vol. 3, no. 10, pp. 2027–2049, 2011, doi: 10.3390/su3102027.
- [18] A. H. Lahuri, A. M. Yusuf, R. Adnan, A. A. Rahim, N. F. Waheed Tajudeen, and N. Nordin, “Kinetics and thermodynamic modeling for CO<sub>2</sub> capture using NiO supported activated carbon by temperature swing adsorption,” *Biointerface Res. Appl. Chem.*, vol. 12, no. 3, pp. 4200–4219, 2022, doi: 10.33263/BRIAC123.42004219.
- [19] A. S. Mahmoud and D. Ph, “Effect of nano bentonite on direct yellow 50 dye removal ; Adsorption isotherm, kinetic analysis , and thermodynamic behavior,” vol. 47, pp. 1–23, 2022, doi: 10.1177/14686783221090377.

# Research into the Possibility of Regenerating Silica Gel using Vacuum

Romana Dobáková<sup>1\*</sup>, Lukáš Tóth<sup>2</sup>

Department of Energy Engineering, Faculty of Mechanical Engineering, Technical University of Košice, Slovakia

\*Corresponding Author

Received: 04 October 2023/ Revised: 10 October 2023/ Accepted: 20 October 2023/ Published: 31-10-2023

Copyright © 2023 International Journal of Engineering Research and Science

This is an Open-Access article distributed under the terms of the Creative Commons Attribution Non-Commercial License (<https://creativecommons.org/licenses/by-nc/4.0>) which permits unrestricted Non-commercial use, distribution, and reproduction in any medium, provided the original work is properly cited.

**Abstract**— Gases used in industry must meet the required technological parameters for the production process, such as the content of gaseous impurities, moisture content and mechanical impurities. Their presence has a significant limiting effect for their further use in technical practice. One of the effective methods of removing moisture from gas is its adsorption, in which the gas passes through a bed of adsorbent, which subsequently binds this moisture on its surface. The article deals with the regeneration of this adsorbent, as it is advantageous from an economic point of view if it is possible to use this adsorbent repeatedly in the gas drying process. By reusing the adsorbent, there is an overall reduction in the cost of operating the equipment and the ecological burden caused by the production of a new adsorbent. The article primarily discusses the influence of the temperature of the dried medium on the speed of its regeneration using vacuum.

**Keywords**— silica gel, adsorption, drying.

## I. INTRODUCTION

The currently growing pressure to reduce energy and production costs forces manufacturers to increase the efficiency of production processes. One of the parameters for achieving the highest possible efficiency of the production process is the use of basic materials with the highest possible purity to prevent unwanted effects during production. Among the most used technical materials in all branches of industry are technical gases, which are subject to strict technical requirements. The amount of moisture contained in these gases indicates their quality. As the amount of moisture contained in the gas increases, its quality decreases and therefore it is necessary to subject them to a drying process.

The drying process is a complicated physical process in which the liquid content of the substance is reduced by the effects of heat, without changing its chemical composition.

The essence of drying is the migration of moisture in the opposite direction to the sorption process. During the general drying process, moisture moves from the porous core of the material to the surface layers and into the surrounding environment, whereupon the moisture meets the drying medium, which carries it away.

To determine the most optimal drying conditions, it is necessary to know the physical laws and quantities that affect drying in the individual phases of the entire process, the input parameters and the required performances.

## II. SILICA GEL AS ADSORBENT

The principle of adsorption is the ability of some porous solid substances to bind gas particles or liquid substances on their surface. The adsorbed amount depends not only on the nature of the adsorbing medium, but also on the nature of the solid substance (adsorbent), on the size of its surface, on the partial pressure of the adsorbing component in the gas phase and on the temperature. During adsorption, it is important that the adsorbent has as large an active surface as possible. Trapped substances are released by desorption and the adsorbent can return to the drying process.

Known adsorbents used in removing moisture from gases include silica gel. It is a granular, porous form of silicon dioxide (SiO<sub>2</sub>), produced synthetically from sodium silicate and sulfuric acid in the form of hard irregular grains or regular balls. The porous structure of interconnected cavities provides a very high surface area (up to 800 m<sup>2</sup>·g<sup>-1</sup>), which allows water vapor to

be easily adsorbed. Ordinary silica gel binds an amount of water corresponding to approximately 20% of its weight. Even when saturated with water vapor, silica gel still has the appearance of a dry product and its shape remains unchanged.

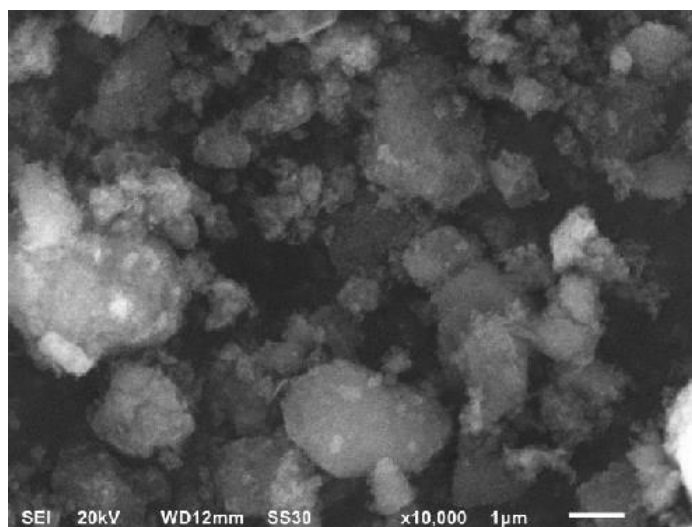


**FIGURE 1: Structure of silica gel [8]**

Silica gel is non-toxic, non-flammable and chemically highly inert. Sometimes it comes with a moisture indicator admixture that will change its colour whenever it is wet.



**a) Type N – normal grains**



**b) Type WS – water resistant grains**



**c) Type Orange gel – indicator grains**

**FIGURE 2: Types of silica gel**

The basic advantage of silica gel is its simple regeneration by increasing the temperature of the adsorbent, which removes the moisture stored in it. A decrease in the energy requirements for such drying can be achieved by reducing the pressure in the system, thanks to which the temperature required to remove moisture from the silica gel will also decrease. Pressure reduction in the adsorbent regeneration system is possible by creating a vacuum. Vacuum drying of silica gel is a suitable drying method, as the lower temperature during regeneration reduces the risk of silica gel degradation. After the drying process, it is necessary to cool the adsorbent in order not to deteriorate its adsorption properties in the gas drying process, as the amount of adsorbed water molecules on its active surface decreases with its increasing temperature.

### **III. DESCRIPTION OF THE MEASUREMENT PROCESS AND DESIGN OF EXPERIMENTAL EQUIPMENT FOR VACUUM DRYING OF SILICA GEL**

An experimental device was designed for the regeneration of silica gel using vacuum drying, including a device for heating the heat-carrying medium and a chamber for humidifying the supplied gas to the drying chamber with silica gel.

For the purposes of the experiment, spherical silica gel EINECS: 231-545-4 was used. Hydrogen with a purity of 99.95% was used as the dried medium.

Fig. 3 shows the basic scheme of the experimental device, which consists of a segment for gas humidification (2), a tank containing silica gel (9), in which the humidified gas is dried, and then a part for heating the heat-carrying medium (5), which serves for regulation temperature in the tank with silica gel. Between the individual parts of this column, there are units for the



analysis of humidity and temperature of the driving gas (1), (8), (11). Resistance thermometers (Thermistor 10K) are placed in the tank with silica gel and in the tank used to heat the water ensuring the required temperature of the silica gel. A vacuum pump (rotary vane pump RE 2.5) is connected to the tank with silica gel, which ensures the required pressure drop during the regeneration process.

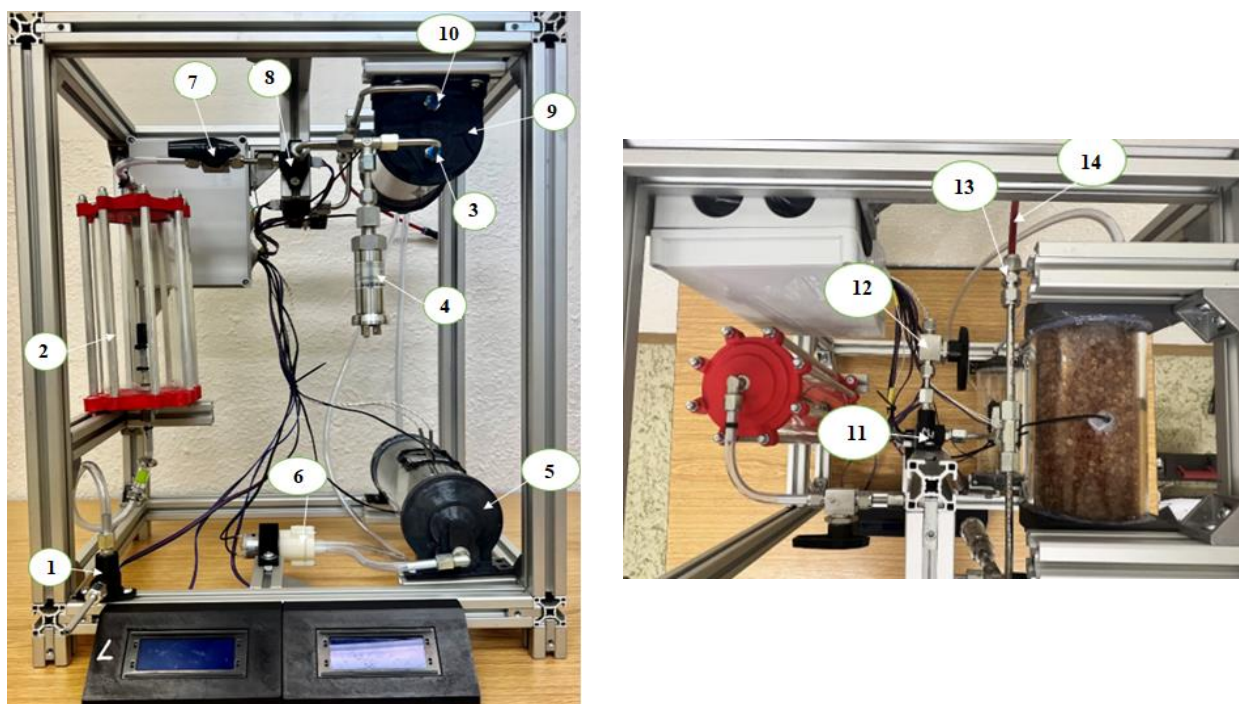


**FIGURE 3: Model of experimental equipment**

(1) (8) - SHT31 sensor (humidity and temperature sensor), (2) - hydrogen humidification chamber, (3) (10) - quick coupling, (4) - DMP331 pressure sensor during vacuuming, (5) - tank with heat exchanger liquid, (6) - pump ensuring water circulation to the container with silica gel, (7) - two-way valve Fitok Boss-ML6-05, (9) - tank with silica gel, (11) - sensor SHT31 (sensing humidity and temperature), (12) - two-way valve Fitok Boss-ML6-05, (13) - quick coupling, (14) - pipe for connecting the vacuum pump

From the pressure tank, the hydrogen is supplied to the humidification chamber, then it flows into the vessel with silica gel, where it dries and is released into the surrounding atmosphere. The heat source located on the tank transfers heat to the water, which circulates with the help of a pump to a spiral placed in a tank with silica gel, where thermal energy is transferred from the water to the adsorbent. After the heat has been transferred, the water returns to the storage tank. After finishing the process of drying wet hydrogen using silica gel, the silica gel regeneration process occurs by closing the circuit for the flow of hydrogen and connecting the vacuum system to the tank with silica gel.

#### IV. EVALUATION OF THE RESULTS FROM THE SILICA GEL REGENERATION PROCESS

Experimental measurement of silica gel regeneration took place in vacuum at four different temperatures (10°C, 25°C, 50°C and 70°C). To achieve a temperature of 10°C in a tank with silica gel, a Peltier cell (PC) with a power of 60 W was used. The PC was placed on an aluminium heat exchanger, which was in a tank with heat exchange liquid. The flow time of moistened hydrogen through the silica gel was the same for all measurements (15 minutes). The hydrogen pressure at the system inlet was set to a constant value to ensure the same volume flow during the measurement period. A constant temperature of the silica gel during the humidification process (approx. 25°C) was also ensured by means of a spiral located in the tank through which the heat-carrying medium flowed. The time to which the silica gel was exposed in the regeneration process was 40 minutes at all four considered temperatures. To determine the moisture removed from the adsorbent during the regeneration process, the silica gel was weighed before vacuuming and during the vacuuming itself. The absolute pressure during vacuuming was maintained at 0.4 bar.

Fig. 4 shows the weight loss of silica gel during vacuum drying at four selected temperatures.

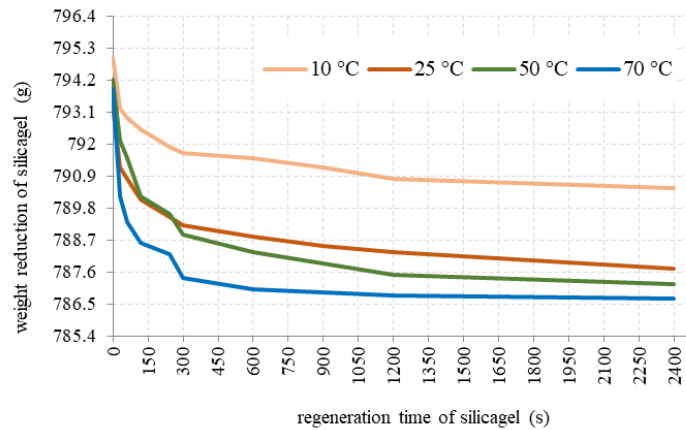


**FIGURE 4: Regeneration of silica gel in vacuum at selected temperatures**

From the graphic dependence, it follows that with the increasing temperature of the silica gel during the process of regeneration with the help of vacuum, there was a significant loss of moisture in it, for the same time interval.

This statement can be clearly confirmed in fig. 5, where at an adsorbent temperature of 70°C during the drying process for 40 min. 7.2 g of moisture taken, while at a temperature of 10°C only 4.5 g.

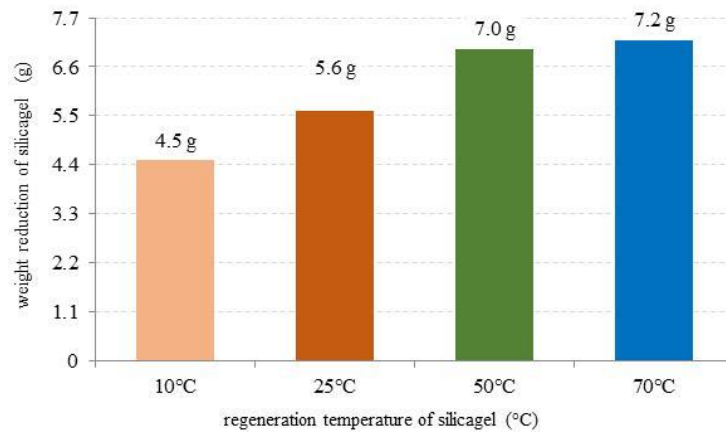


**FIGURE 5: Loss of moisture in silica gel during its regeneration in vacuum at selected temperatures**

In fig. 6, the time required for silica gel regeneration at 25°C and 70°C is investigated. From the dependence, it follows that at a temperature of 25°C, the adsorbent needs to be dried for up to 90 min to achieve a dryness comparable to that in the case of regeneration at a temperature of 70°C.

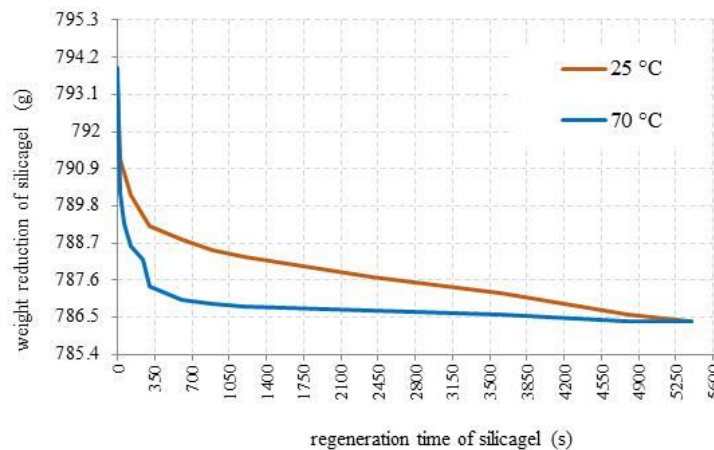


**FIGURE 6: Comparison of the time required for the regeneration of silica gel at temperatures of 25°C and 70°C**

Drying silica gel at higher temperatures, not only in a vacuum, ensures faster desorption of water molecules from its active surface. Regeneration of silica gel in a vacuum takes place faster compared to classic drying processes, as the amount of removed moisture per unit of time also increases by reducing the pressure in the system.

## V. CONCLUSION

Vacuum drying wet material can significantly reduce its drying time due to the low-pressure environment. This lowers the boiling point of water, which accelerates the removal of free and bound moisture from the dried material. Thanks to lower temperatures, this method of regeneration prevents thermal damage or material degradation.

From the experiments presented in the article, it follows that vacuum drying is ideal for the desorption of moisture from silica gel at a temperature of 70°C, as the moisture bound on its surface is released faster. Lowering the temperature also results in an increase in the time required for the regeneration of the silica gel and its reintroduction into the gas drying process.

When designing a device used for the regeneration of silica gel using a vacuum, it is also necessary to consider the economic aspects of drying, as the provision of a vacuum system can mean significant financial costs, but the reduction of the drying temperature compared to classical methods gives the possibility of saving energy spent in the process of regeneration of silica gel.

## ACKNOWLEDGEMENTS

This paper was written with the financial support from the VEGA granting agency within the Projects No. 1/0224/23 and No. 1/0532/22, from the KEGA granting agency within the Project No. 012TUKE-4/2022, and with the financial support from the APVV granting agency within the Projects No. APVV-15-0202, APVV-20-0205 and APVV-21-0274.

## REFERENCES

- [1] Čiahotný, K., Černá, E., Macháčková, M.: *Testování adsorbentů pro separaci oxidu uhličitého z plynů*. Chemické listy, 107 (2013), p. S. 555–560.
- [2] Grande, C. A. et. al.: *Silica Gel as a Selective Adsorbent for Biogas Drying and Upgrading*. Ind. Eng. Chem. Res, 59 (2020), p. 10142–10149.
- [3] Mourik, J.: *Experiences with Silica Gel as Adsorbent*. American Industrial Hygiene Association Journal, 26 (5) (2007), p. 498 – 509.
- [4] Scherer, G. W.: *Effect of drying on properties of silica gel*. Journal of Non-Crystalline Solids, 215 (2-3) (1997), p. 155 -168.
- [5] Mujumdar, A.S.: *Principles, Classification, and Selection of Dryers*. Handbook of Industrial Drying. CRC, (2006). p. p. 1279.
- [6] Du, D.; Jiang, Y.; Feng, J.; Li, L.; Feng, J.: *Facile synthesis of silica aerogel composites via ambient-pressure drying without surface modification or solvent exchange*. Vacuum, 173, (2019), 109117.
- [7] Yan, K. L. and Wang, Q.: *Adsorption characteristics of the silica gels as adsorbent for gasoline vapors removal*. IOP Conf. Series: Earth and Environmental Science, 153 (2018), 022010.
- [8] Song, Z., Zhao, H.: *Preparation and Characterization of Mullite-Silica Aerogel Composite Material*. Open Journal of Organic Polymer Materials, 8 (4) 2018, p. 43 – 52.

# Structural Design of Atypical Metal hydride Tank and Investigation of Generated Temperature Fields: Part I

Filip Duda<sup>1\*</sup>, Natália Jasminská<sup>2</sup>

Department of Energy Engineering, Faculty of Mechanical Engineering, Technical University of Košice, 042 00 Košice, Slovak Republic

\*Corresponding Author

Received: 06 October 2023/ Revised: 12 October 2023/ Accepted: 21 October 2023/ Published: 31-10-2023

Copyright © 2023 International Journal of Engineering Research and Science

This is an Open-Access article distributed under the terms of the Creative Commons Attribution Non-Commercial License (<https://creativecommons.org/licenses/by-nc/4.0>) which permits unrestricted Non-commercial use, distribution, and reproduction in any medium, provided the original work is properly cited.

**Abstract**— The article describes the structural design of an atypical metal hydride storage tank for hydrogen storage for mobile operations such as cars, buses, etc. The structural design of the tank consists of three main parts, namely an atypical bottom of an elliptical shape with a flange on which there is a 1/4NPT" thread, three seamless pipes and a second atypical bottom as a cap. Hydrogen storage works under low pressure of up to 30 bars and is based on TiFe alloys. In the next part, the article deals with the investigation of the temperature fields created in an atypical metal hydride tank, and then it is devoted to an effective method of cooling the metal hydride tank during the process of hydrogen absorption into the structure of the metal alloy.

**Keywords**— Metal hydride, pressure tank, heat transfer.

## I. INTRODUCTION

Storage of hydrogen in high-pressure composite tanks with compressed gas (CGH<sub>2</sub>) at pressures from 350 to 700 bar is the most common method of supplying hydrogen to fuel cells. This solution has the advantages of relatively high hydrogen storage capacity, short refueling time (3-5 min) and virtually unlimited flow of hydrogen into the fuel cell. However, the volume capacity of hydrogen storage by the CGH<sub>2</sub> system is too low. These systems also suffer from problems, namely: low safety and extremely expensive refueling infrastructure - both problems are associated with the high pressure of the stored hydrogen.

Metal hydrides (MHs) formed by the reversible reaction of gaseous H<sub>2</sub> with a parent metal, alloy, or intermetallic compound to form a hydride are particularly promising for hydrogen storage. The use of MH can provide very high hydrogen storage capacity per unit volume (sometimes higher than liquid hydrogen), safety, reliability and high purity of supplied H<sub>2</sub>. Despite the conventional view of the low weight hydrogen storage capacity of "low temperature" intermetallic hydrides ( $\leq 2$  wt.% H) as their main drawback in on-board hydrogen storage systems, in some special applications in vehicles the use of these materials appears to be very promising. Primarily this applies to material handling units, underground mining vehicles and water applications where the low gravimetric hydrogen storage capacity/high mass of metal hydrides can provide advantages in vehicle/vessel stabilization.

For this method of hydrogen storage to be used as effectively as possible, it is necessary to design the tank in such a way that it meets all operational parameters in terms of strength. It is also necessary to design an efficient cooling system of the tank during the process of hydrogen absorption into the structure of the metal alloy. This article discusses the solution to the structural design of an atypical metal hydride tank, as well as the design of effective cooling.

## II. STRUCTURAL DESIGN OF AN ATYPICAL METAL HYDRIDE STORAGE TANK

The tank consists of three main parts, namely an atypical bottom of a rectangular shape, on which there are two holes with 1/4 NPT" thread, which serve for the supply of hydrogen to the MH tank, three seamless pipes and a second atypical bottom serving as a cap of the tank. In all pipes there is a heat transfer intensifier, which serves to effectively remove the heat generated during the process of hydrogen absorption into the structure of the metal alloy. The heat that is released during the process of hydrogen absorption into MH is approximately 1 MJ per 1 m<sup>3</sup> of stored hydrogen. The material from which the intensifier is made is aluminum, because it has good thermal conductivity ( $\lambda=237$  W·m<sup>-1</sup>·K<sup>-1</sup>).

All main parts of the atypical metal hydride tank are made of stainless steel 316L-1.4404. It is a type of steel, that is compatible for hydrogen applications and chosen based on the STN EN 13322-2 standard. The mechanical properties of the steel used are listed in Table 1, the operating parameters of the designed tank are shown in Table 2. The structural design of the tank can be seen in Fig. 1.

**TABLE 1**  
**MECHANICAL PROPERTIES OF STAINLESS STEEL 316L-1.4404**

0.2% Re (MPa)	Rm (MPa)	$\rho$ (kg·m <sup>-3</sup> )	$\mu$	E (MPa)
205	515	7950	0.3	$2.1 \cdot 10^5$

Where: *Re*-yield strength, *Rm*-strength strength,  $\rho$ -density,  $\mu$ -Poisson's number and *E*-Young's modulus of elasticity.

**TABLE 2**  
**PARAMETERS OF THE DESIGNED VESSEL**

The weight of the empty vessel	5.71 kg
Weight of metal hydride	8.5 kg
Total weight of the vessel with MH	14.2 kg
Metal hydride volume	$3 \cdot 10^{-3}$ m <sup>3</sup>
Mass of stored hydrogen	0.116 kg
Volume of hydrogen	1.38 m <sup>3</sup>
Generated heat	13867.8 kJ

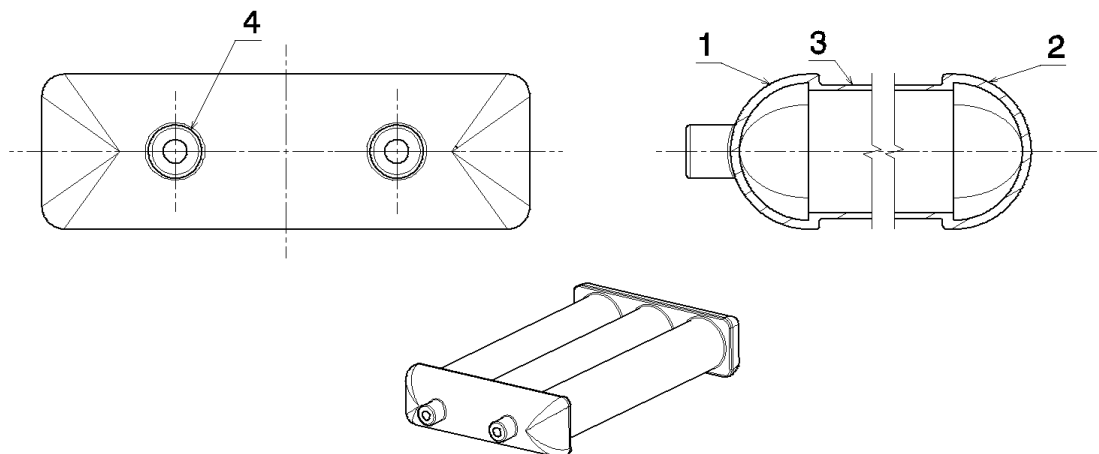


**FIGURE 1: Structural design of an atypical metal hydride storage tank**

Where 1- an atypical bottom of a rectangular shape with a hole for a flange, 2- an atypical bottom as a tank cap, 3- a cylindrical seamless pipe.

The control strength calculation of the designed tank solved in the Ansys Static Structural program showed that the maximum stress according to the Von Mises theory did not exceed the values higher than the yield strength *Re* according to Table 1 and the resulting stress on the tank was approximately 120 MPa at an operating pressure of 3 MPa, which means that the tank it is designed well enough for the given operating parameters.

### III. SIMULATION OF HEAT TRANSFER OF THE DESIGNED ATYPICAL TANK

The simulation is solved using the FEM method, where the problem of heat transfer from the tank core is solved. In this simulation, a 3D model of the designed tank, in which the metal hydride alloy is located, is considered. The simulations were divided into three, where in the first simulation the tank was not cooled, in the second simulation the cylindrical parts of the metal hydride tank are immersed in water, which represents active cooling, and in the third simulation passive cooling in the

form of heat transfer intensifiers, which are located in cylindrical seamless pipes, is considered and active cooling, where the tank, as in the second simulation, is immersed in the cooling liquid.

### 3.1 Setting up the First Simulation:

In the first simulation, the maximum temperature that arises in the tank during the process of hydrogen absorption into the structure of the metal alloy is investigated. The entire process of hydrogen absorption takes 20 min, which also represents the total time of the simulation. The simulation was performed in the ANSYS CFX program, where at the beginning it was necessary to set all the boundary conditions as well as to generate the mesh of finite elements. The finite element mesh of the simulation model consists of approximately 1,200,000 volume finite elements with quadratic approximation and 6,000,000 nodes. The mesh of finite elements of the simulation model is shown in Fig. 2. The initialization temperatures of the environment in which the tank is located, the tank itself and the metal hydride alloy were set to 20 °C. The power of the generated heat in the metal hydride alloy during the hydrogen absorption process is set to  $107 \cdot 10^3 \text{ W} \cdot \text{m}^{-3}$ . Before starting the simulation, it is necessary to identify the individual domains of the tank and assign the selected material properties to them. These include a steel tank and a metal hydride alloy, and it is necessary to define the connection between the defined domains.

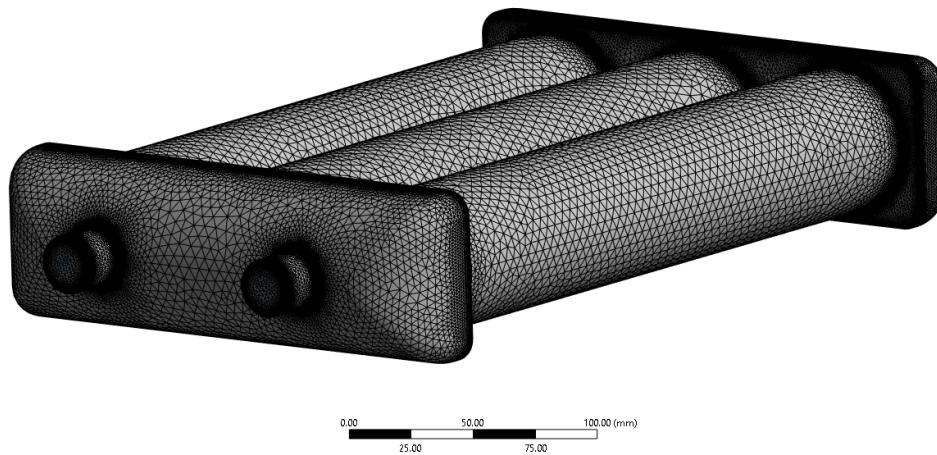


FIGURE 2: Finite element mesh of the first simulation

### 3.2 Results of the First Simulation:

The simulation showed that the maximum temperature in the tank during the process of hydrogen absorption into the metal alloy structure, which lasted 20 min, is approximately 49.5 °C. The result of the simulation is shown in Fig. 3.

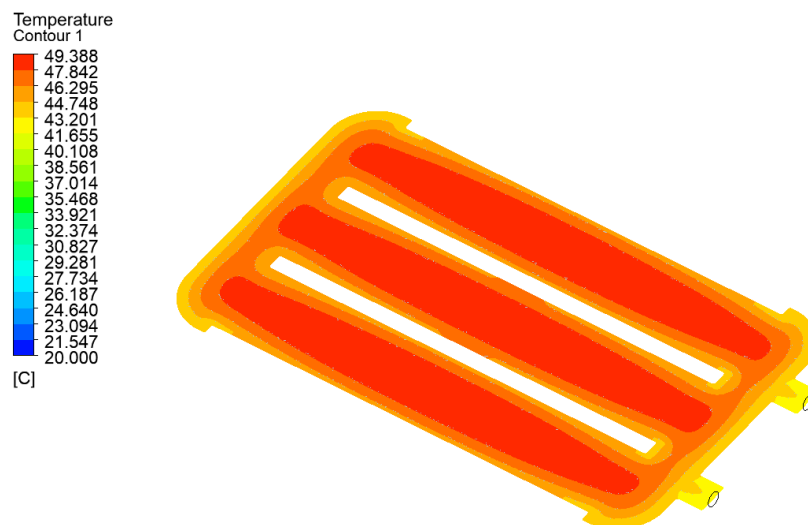


FIGURE 3: Maximum temperatures on the tank during the process of hydrogen absorption into the metal alloy structure without the use of a cooling system

For the kinetics of hydrogen absorption to be higher, it is necessary to cool the metal hydride tank and therefore it is necessary to design an effective cooling system so that the generated heat is removed from the tank as efficiently as possible.

### 3.3 Setting up the Second Simulation:

In the second simulation, the maximum temperature that arises in the tank during the process of hydrogen absorption into the metal alloy structure is investigated, while the cylindrical tubes are immersed in water at a temperature of 20 °C, which represents active cooling. The simulation time is set as in the first simulation to 20 min. The finite element mesh of the simulation model consists of approximately 1,400,000 volume finite elements with quadratic approximation and 6,500,000 nodes. The mesh of finite elements of the simulation model is shown in Fig. 4. The boundary conditions of this simulation have the same settings as in the previous simulation. Before the simulation, it is necessary to define the domains of the simulation model, assign the material used to them as in the previous simulation and set the connection between the individual domains. In this simulation, there are three domains: steel tank, metal hydride alloy and water.



FIGURE 4: Finite element mesh of the second simulation

### 3.4 Results of the Second Simulation:

The simulation showed that the maximum temperature in the tank during the absorption process was reduced to about 42 °C. The result of the simulation is shown in Fig. 5.

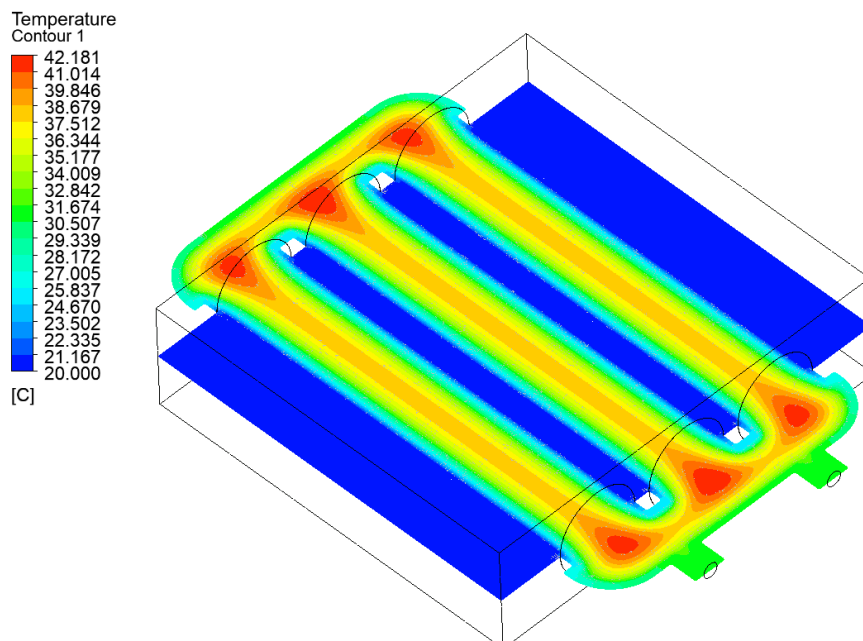


FIGURE 5: Maximum temperatures during the process of hydrogen absorption into the metal alloy structure using active cooling on cylindrical pipes.

For the heat to be dissipated even more efficiently and thus the kinetics of hydrogen absorption to be higher, it is necessary, for example, to insert a heat transfer intensifier into the cylindrical pipes.

#### IV. CONCLUSION

The task of this work was to design a metal hydride tank for storing hydrogen of an atypical shape for mobile applications. Another task of the work was the investigation of the occurrence of maximum temperatures in the tank during hydrogen refueling and subsequently the proposal of effective cooling for the designed tank.

In the first simulation, where no cooling was used, the maximum temperature in the tank was around 49.5 °C. Subsequently, after applying active cooling to the seamless pipes of the designed metal hydride reservoir, the temperature was reduced to approximately 42 °C, thanks to which the kinetics of hydrogen absorption into the metal hydride alloy increases.

Another task of this work will be to design a suitable shape of the internal heat transfer intensifier, for the most effective heat transfer to the inner wall of the steel tank, where this heat will be cooled by active cooling, which would further reduce the maximum temperature of the metal hydride alloy and which would significantly increase the kinetics of absorption hydrogen.

#### ACKNOWLEDGEMENTS

This paper was written with financial support from the VEGA granting agency within the project's no. 1/0224/23 and no. 1/0532/22, from the KEGA granting agency within the project no. 012TUKE-4/2022 and with financial support from the APVV granting agency within the projects no. APVV-15-0202, no. APVV-20-0205 and no. APVV-21-0274.

#### REFERENCES

- [1] Afzal, M. Mane, R. Sharma, P.: Heat transfer techniques in metal hydride hydrogen storage: A review. *International Journal of Hydrogen Energy* 42, 2017.
- [2] Chibani, A. Bougriou, Ch. Merouani, S.: Simulation of hydrogen absorption/desorption on metal hydride LaNi<sub>5</sub>-H<sub>2</sub>: Mass and heat transfer. *Applied Thermal Engineering* 142, 2018.
- [3] Valizadeh, M. Delavar, A, M. Farhadi, M.: Numerical simulation of heat and mass transfer during hydrogen desorption in metal hydride storage tank by Lattice Boltzmann method. *International Journal of Hydrogen Energy* 41, 2016.
- [4] Jurczyk, Mieczyslaw.: *Handbook of Nanomaterials for Hydrogen Storage*. Singapore: Pan Stanford Publishing Pte. Ltd, 2018. ISBN 978-1-315-36444-5.
- [5] Lipman, E. T., Weber, Z, A. *Fuel Cells and Hydrogen Production*. New York: Springer Science+Business Media, 2018. ISBN 978-1-4939-7789-5.
- [6] Stolten, D. (2010). *Hydrogen and Fuel Cells*, Weinheim: Wiley, 2010, 908 p. ISBN 978-3-527-32711-9.
- [7] Brestovič, T., Jasminská, N. *Numerické metódy a modelovanie v energetike*, Košice, Sjf TU v Košiciach, 2015. ISBN 978-80-553-0223-2.



# Gas Transmission System Optimization with Natural Gas Transportation

Ľubomíra Kmeťová

Department of Energy Engineering, Faculty of Mechanical Engineering, Technical University of Košice, Slovakia

\*Corresponding Author

Received: 06 October 2023/ Revised: 17 October 2023/ Accepted: 24 October 2023/ Published: 31-10-2023

Copyright © 2023 International Journal of Engineering Research and Science

This is an Open-Access article distributed under the terms of the Creative Commons Attribution Non-Commercial License (<https://creativecommons.org/licenses/by-nc/4.0>) which permits unrestricted Non-commercial use, distribution, and reproduction in any medium, provided the original work is properly cited.

**Abstract**— In connection with the heated political situation to the east of the European Union (EU) borders, there is a growing interest in the discovery of new reserves of natural gas or new suppliers of this fossil fuel. This situation consequently requires new and unconventional ways of solving the storage and transportation of gas in large quantities and over long distances. The following article discusses the methods of storage and transportation of natural gas through the gas network.

**Keywords**— Natural Gas, Storage Tanks, Pipelines, Compressors Station.

## I. INTRODUCTION

Natural gas consumption is uneven throughout the year, it can fluctuate, and therefore the gas is stored. In addition to natural gas reservoirs and gas pipelines, the gas system consists of several important parts and components.

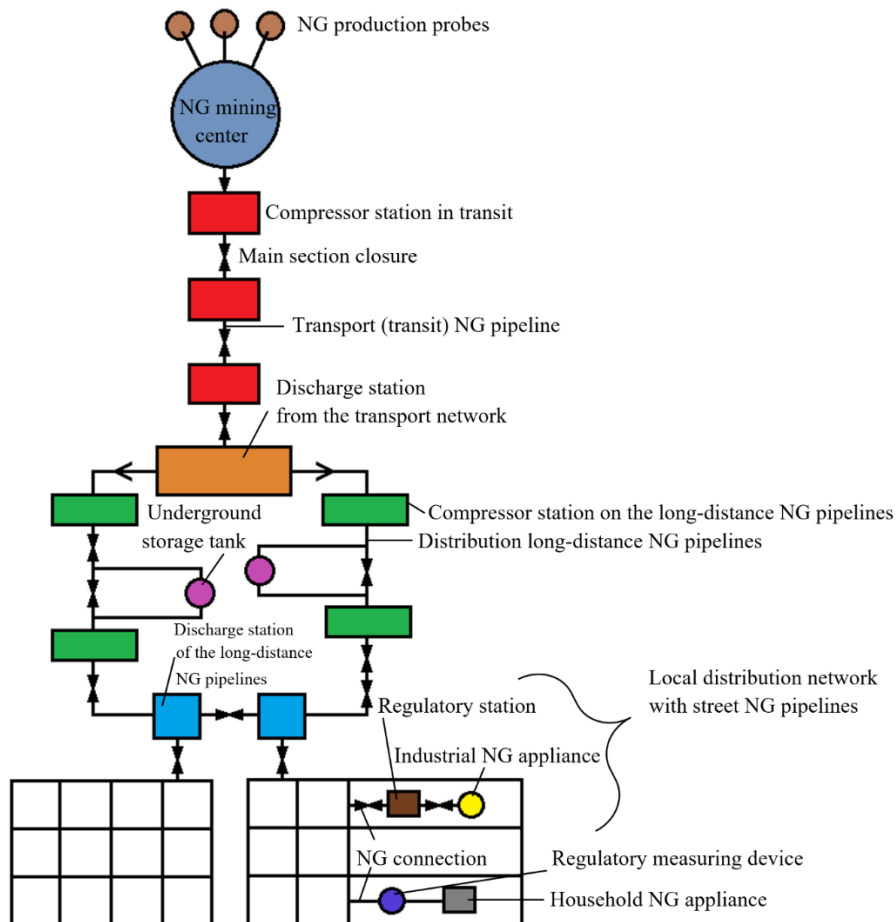


FIGURE 1: Diagram of the transport and distribution natural gas (NG) system [1]

## II. NATURAL GAS STORAGE

Natural gas stored in storage facilities meets the requirements of seasonal demand and serves as insurance against unpredictable gas supply interruptions.

The basic storage capacity is used to increase seasonal demand. Baseload facilities can hold enough natural gas to meet long-term seasonal demand requirements.

The turnover rate of natural gas in storage tanks is one year. Natural gas is injected into storage tanks during the summer (outside of the heating season), usually from April to October. Seasonal reservoirs are more voluminous, but their daily output is relatively low and limited.

Tanks are built for all types of heating gases. There are above ground or underground storage tanks of various sizes and types.

Natural gas, like most other commodities, can be stored indefinitely. Exploration, extraction, and transportation of natural gas take time. Natural gas, which is transported to its destination and is not always used for immediate consumption, is injected into underground reservoirs. Consumption is significantly higher during the winter, as natural gas is mainly used for heating.

Strategically, underground storages of natural gas are used for seasonal regulation, which means compensating for increased gas consumption in the winter season by extracting it from storage tanks in which gas is stored in the summer season, when consumption is lower. They are efficient from a financial point of view because the purchase of gas takes place during the period when gas prices are lower, its storage and subsequent extraction during the period of higher prices. At the same time, they ensure the safety of deliveries in case of production or transport disruptions. These reservoirs have a large storage capacity, but a smaller daily output.

Tanks that are used for peak loads are designed to have high performance in a short time, which means that natural gas can be quickly withdrawn from the tank if needed. Peak load devices are designed for sudden increases in short-term demand. These devices are not as bulky as baseload devices, but they can deliver a smaller amount of gas faster and in less time than baseload devices. In contrast to seasonal reservoirs, these reservoirs can be refilled to their maximum capacity during the winter period.

Geological structures suitable for the creation of underground reservoirs must mainly meet the following geological-deposit criteria:

- Gas Tightness of The Formation,
- Effective Porosity,
- Size of Usable Cubic Capacity,
- Storage Depth.

On a global scale, the most used type for the creation of underground reservoirs are the natural gas and oil extracted deposits. If such sites are not available, storage tanks are built in watered layers of the so-called aquifer type. These types of reservoirs have a large storage capacity but a smaller daily output and are referred to as seasonal reservoirs.

Peak reservoirs are most often established in salt caverns (cavities), which are created by treating part of the salt deposit with water. Less often, other underground cavities are used for this purpose, such as abandoned coal or ore mines or artificially cut caverns.

With underground reservoirs, we recognize the prospective need for the stored amount of gas, i.e., the required storage capacity and the ready mining capacity.

The most common form of underground reservoirs is porous (Figure 2). These are mostly extracted deposits of oil or natural gas that are used to re-store the gas, leaving an underground formation geologically capable of holding natural gas.

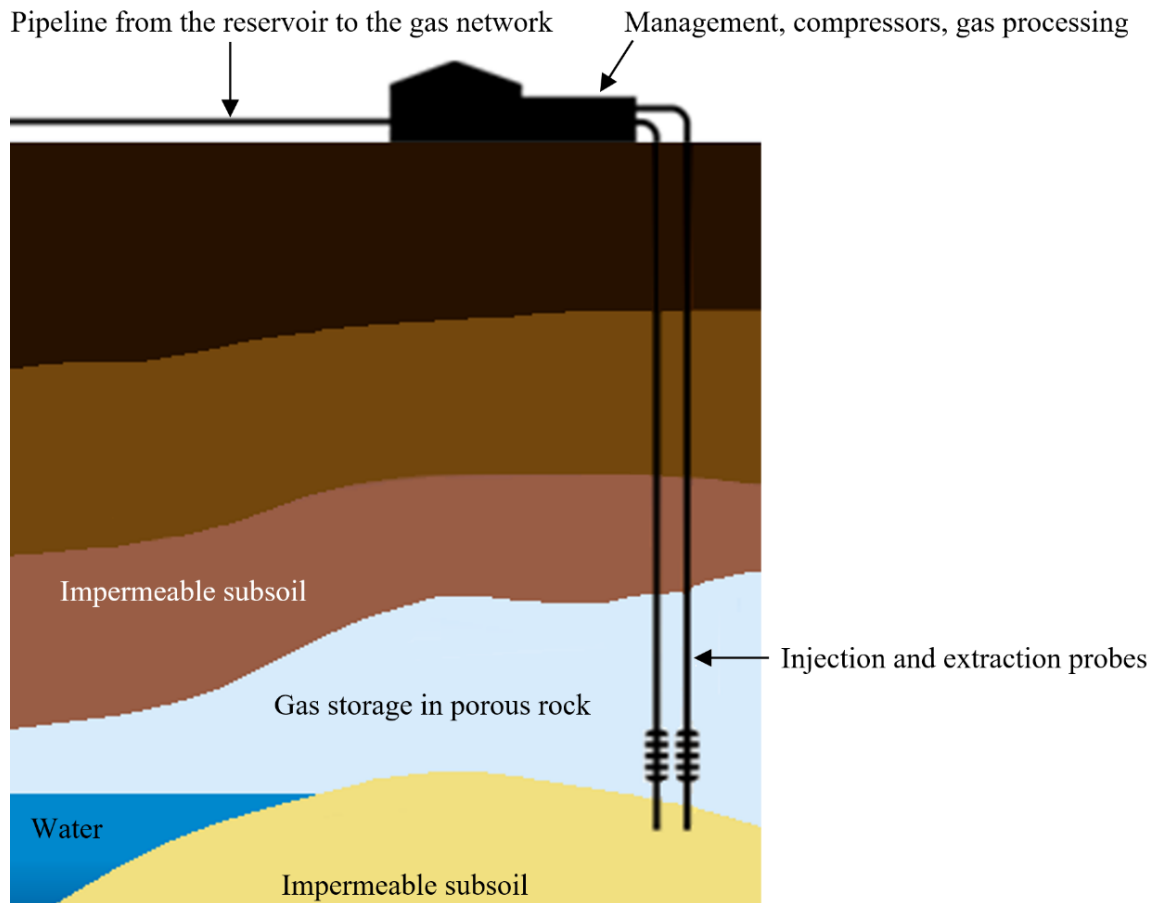


**FIGURE 2: Porous NG storage [2]**

Exhausted deposits are attractive also because their geological characteristics are already well known. The gas is stored in porous rocks, which are most often formed by sandstone and various consolidated sands containing clay.

### III. TRANSIT SYSTEM OF NATURAL GAS

As already mentioned, the discovery of large-capacity natural gas deposits on various continents and the appreciation of the importance of natural gas in its wide range of uses as an energy source and raw material laid the foundations for transportation systems.

The basic characteristics of the natural gas transmission system are:

- Verified Large-Capacity Gas Deposits,
- Transportation of Large Quantities of Gas (on the order of billions  $m^3$  per year),
- Large Diameter Pipes Consisting of Several Lines (approx. 900 to 1,400 mm),
- High Operating Transport Pressures (5 to 7.5 MPa),
- Long Linear Lines Connecting the National Gas Systems of the Individual States of the Continent (Thousands of km).

In terms of the relevant legislation, the transport NG network is characterized as a network of compressor stations and a network of mainly high-pressure gas pipelines, which are connected to each other and serve to transport NG in a defined area, in addition to the extraction network and storage and high-pressure NG pipelines, which serve primarily to transport NG in parts of the defined area.

The natural gas transportation system consists of:

- Border Discharge Stations,
- Pipelines,
- National Discharge Stations,
- Compressor Stations.

#### IV. PIPELINES

At the beginning of the transportation chain, when it is necessary to transport large volumes of natural gas over long distances, natural gas is most often transported in two basic ways: gas pipelines or in tankers in the form of liquefied gas.

By gas pipeline, we understand the system of pipes through which we transport natural gas from the place of extraction to the place of consumption. As the consumption of natural gas grew in the past, deposits near large cities were gradually exploited, so it was necessary to transport natural gas over greater distances and in larger volumes. Long-distance gas pipelines are run not only on land, but also on the seabed, which makes it possible to transport natural gas also from other continents.

There are several types of gas pipelines:

- Transit Transmission Lines,
- Distribution (Connecting) Transmission Lines.

The task of transit transmission lines is to transport a large amount of heating gases, usually natural gas, from mining deposits over distances of several hundred kilometers to the area of main consumption. National or interstate transmission lines usually have a pipe diameter of over 500 mm and an operating pressure of over 5 MPa.

Distribution (connecting) long-distance lines ensure gas transport from the main transit arteries to individual gas-supplied areas and interconnected and circularized ensure smooth gas supply to customers. As a rule, they are built under 500 mm pipe diameter and under 5 MPa operating pressure, their lengths are usually a few hundred kilometers at most. Depending on the operating pressure, they can create separate distribution circuits.

An important part of the transit transmission lines are route closures (Figure 2), which are placed approximately every 20-25 km. They enable possible stopping of the gas flow on individual sections of the gas pipeline. When the transported amount of gas drops, the valve closes automatically and closes the section. Other functions of the route closures are, for example, the depressurization of the gas pipeline, the release of gas between gas pipeline sections and eventual cleaning of gas pipeline sections.

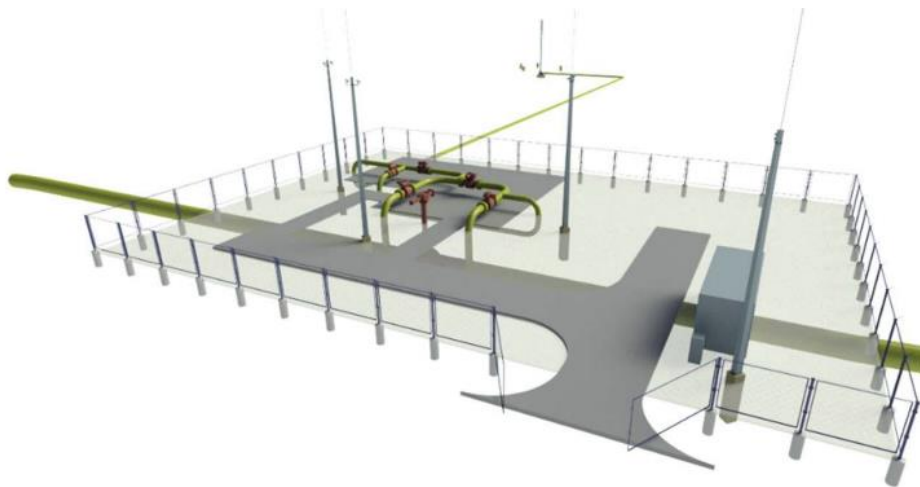


**FIGURE 3: Route closure [3]**

#### V. COMPRESSOR STATIONS

As a rule, the extraction technology from deposits does not allow using the deposit pressures to transport large quantities of natural gas through long-distance transit pipelines to places of consumption.

When transporting natural gas through long-distance gas pipelines, pressure losses occur. These losses are caused by the friction of the gas both against the walls of the pipe and by the internal friction of the individual parts of the gas against each other. Pressure losses must be compensated to deliver the gas to the designated location. Compressor stations as part of gas pipelines serve this purpose - they increase gas pressure. For safety and operational reasons, they are built outside cities and towns.

The station consists of a system of interconnected devices that can be divided into two groups:

- Equipment serving its own gas compression and gas treatment equipment (compressors, compressor drives, pipelines, filters, gas coolers),
- Service facilities (energy and oil management, firefighting equipment, laboratories, and workshops).

Compressors used in the gas industry are divided into two basic groups:

- Reciprocating Compressors,
- Turbo Compressors.

Reciprocating compressors work based on the change in the volume of the working space (cylinder).

Turbochargers are high-speed machines in which the pressure increases due to the increase in the velocity of the gas flowing between the rotor blades.

The largest compressor station in the territory of the European Union is the Veľké Kapušany compressor station (Figure 4), located in Slovakia. The technical capacity at the entry point in Veľké Kapušany is 220 million cubic meters of natural gas per day. [4]

Gasification in Slovakia began in 1951, when the first gas pipeline was built on the territory of today's Slovakia, which was 38 kilometres long. Between 1970 and 1973, a parallel transit pipeline with a huge annual capacity of 28 billion m<sup>3</sup> was built to transport gas to Germany. Currently, up to 94% of the population in Slovakia has access to natural gas.



**FIGURE 4: Largest EU compressor station in Slovakia [5]**

## VI. CONCLUSION

The costs of construction, operation, or modernization of the gas network together with natural gas storages represent a significant investment for their developer or operator. The time required for construction plays an equally important role. It is therefore necessary to carefully consider the use of currently existing networks as well as storage facilities as well as the construction of new ones.

New deposits and new forms of natural gas transportation, as well as the search for new sources of energy, could bring about a stable operation of the world economy again in the future without deepening the ongoing climate change.

## ACKNOWLEDGMENTS

This paper was written with financial support from the VEGA granting agency within the projects no. 1/0224/23 and no. 1/0532/22, from the KEGA granting agency within the project no. 012TUKE-4/2022 and with financial support from the APVV granting agency within the projects no. APVV-15-0202, no. APVV-20-0205 and no. APVV-21-0274.

## REFERENCES

- [1] RAPČÍK, M., SMOLA, M., BOHÁČ, M., MUCHA, M. (2004). Fundamentals of Energy. Part I. Slovak Technical University in Bratislava. 2004. 204 p. ISBN 80-227-2074-7.

- [2] SPP Storage. <<https://www.sppstorage.cz/en/dolni-bojanovice-ugs-facility/types-of-underground-gas-storage-facilities/>>. (Accessed 08.09.2023)
- [3] MATULA, T. (2018). Eastring: Feasibility Study: Results & Recommendations. <<http://ceec.sk/ppt/Matula.pdf>>. (Accessed 08.09.2023)
- [4] EUSTREAM Company: Natural Gas Network Development Plan for Years 2020 – 2029. 29 p. <[https://www.eustream.sk/files/sk/transparency/rozvoj-siete/plany-rozvoja-siete/eus\\_tyndp\\_2020\\_2029.pdf](https://www.eustream.sk/files/sk/transparency/rozvoj-siete/plany-rozvoja-siete/eus_tyndp_2020_2029.pdf)>. (Accessed 08.09.2023)
- [5] Photo documentation of the compressor station in Slovakia. <<https://www.cas.sk/fotogaleria/292253/vynimocny-den-pre-europu-ukrajinu-i-slovensko-fico-a-jacenuk-symbolicky-spustili-reverzny-tok-plynu/1/>>. (Accessed 08.09.2023)
- [6] FÍK, J. (2006). Natural Gas. 1st. Edition. Agentura ČSTZ, s.r.o., Praha, 2006. 357 p. ISBN 80-86028-22-4.
- [7] BOYUN GUO and ALI GHALAMBOR. Natural Gas Engineering Handbook. 2012. ISBN 978-1-933762-41-8.
- [8] DOBÁKOVÁ, R., JASMINSKÁ, N., KMEŤOVÁ, L., LÁZÁR, M. Plynárenské zariadenia. 1st. Edition. Košice: Technical University of Košice. 2022. 266 p. [CD-ROM]. ISBN 978-80-553-4165-1.

# Design of A Model of Liquid Feeder to an Incinerator of Hazardous Waste and its Optimization from the Cooling Point of View: Part I

Ivan Mihálik<sup>1\*</sup>, Marián Lázár<sup>2</sup>, Tomáš Brestovič<sup>3</sup>

Department of Energy Engineering, Faculty of Mechanical Engineering, Technical University of Košice,  
Vysokoškolská 4, 042 00 Košice, Slovakia

\*Corresponding Author

Received: 07 October 2023/ Revised: 15 October 2023/ Accepted: 26 October 2023/ Published: 31-10-2023  
Copyright © 2023 International Journal of Engineering Research and Science

This is an Open-Access article distributed under the terms of the Creative Commons Attribution Non-Commercial License (<https://creativecommons.org/licenses/by-nc/4.0>) which permits unrestricted Non-commercial use, distribution, and reproduction in any medium, provided the original work is properly cited.

**Abstract**— A series of articles aimed at the cooling of the liquid radioactive waste feeder into the incinerator space optimization. The first part of the article offers a theoretical analysis of radioactive waste and the possibilities of its incineration. It also deals with the heat transfer within the waste feeder by means of the criterion equations for the transverse flow around the pipe at an angle, thanks to which the required mass flow of the cooling medium is determined.

**Keywords**— Hazardous Waste, Radioactive Waste, Heat Transfer, Cooling Optimization.

## I. INTRODUCTION

A significant amount of waste is produced in the energy industry. These wastes are divided into several types according to the possibility of their further processing. For example, common waste can be recovered for energy or stored, and hazardous waste must be disposed of. A specific branch of the energy industry is nuclear energy. Radioactive waste is generated during the operation of a nuclear power plant. Safe storage of this waste is spatially and financially demanding. For this reason, volume reduction of radioactive waste is necessary before its further processing.

Some types of radioactive waste can be burned in an incinerator to minimize its volume. The resulting radioactive ash is then safely stored for a long time. The incinerator is equipped with a dowerm and ionex feeder. It is necessary to effectively cool this feeder to maintain the limited working temperature of the ionex and thereby ensure problem-free operation.

## II. TYPES OF RADIOACTIVE WASTE ACCORDING TO RADIOACTIVITY

Radioactive waste is generated not only during the operation of nuclear power plants, but also, for example, within medical and research facilities, in agriculture and in services. In general, the term radioactive waste refers to waste materials that, due to the high content of radionuclides, or due to irremovable contamination, cannot be further used, recycled and released into the environment. Radioactive waste can be divided into many categories based on their chemical, physical and radiochemical properties. The most common division of these wastes is based on their level of radioactivity and state. According to the degree of radioactivity, waste can be divided into low-level waste, intermediate-level waste and high-level waste.

Low-level waste contains a significant amount of only short-lived radionuclides. Their decomposition to a sufficiently low level usually takes only a few decades. Low-level waste includes waste consisting of various materials and states. These are, for example, parts of protective equipment for nuclear power plant workers, such as gloves and coats. Low-level waste makes up approximately 90% of total radioactive waste. A large part of this waste can be classified as combustible waste, which makes it possible to reduce the total volume of waste to a large extent.

Intermediate-level waste contains significant quantities of long-lived radionuclides which do not generate significant decay heat. These are wastes from industrial facilities and institutional radioactive wastes, which, after reducing their volume, can be further stored in a multi-barrier protection system, or safely disposed of.

High-level waste consists of  $\alpha$ -emitters and waste arising from fission products of uranium fuel in the reactor. Most high-level waste results from the reprocessing of spent nuclear fuel. If the nuclear reactor fuel that has been removed from a reactor following irradiation is treated as a waste, it is also considered a type of high-level waste. This type of radioactive waste is characterized by a high level of radioactivity and also radiotoxicity. Spent nuclear fuel contains more than 1000 radionuclides. It is essential to prevent these nuclides from entering the environment for an extremely long period of thousands of years. In order to achieve a decrease in the radioactivity and thermal output of high-level waste, it is necessary to cool the fuel for a period of 3 to 5 years. Subsequently, the cooled fuel can be moved and stored for up to 50 years in spent fuel interim storage. After the decrease in radioactivity and residual heat output, it is possible to definitively store the waste in a deep repository.

### III. TYPES OF RADIOACTIVE WASTE ACCORDING TO STATE

According to its state, radioactive waste is divided into solid, liquid and gaseous. Solid radioactive waste can be created in two ways. The first is activation by the direct influence of radioactive radiation, when solid materials themselves become emitters. The second way is the contamination of solid materials in contact with active media, for example with the cooling medium of the primary circuit. Some contaminated components and equipment, such as primary circuit piping, can continue to operate. Other equipment and tools that may come into contact, for example, with power plant workers, must be decontaminated. Some contaminated materials, such as various filters, measuring devices, laboratory aids and others, are no longer usable due to their high activity. Contaminated elements of the building structure of the power plant are specific radioactive waste. It must be disposed of only when the power plant is decommissioned.

The liquid wastes generated during the operation of the nuclear power plant have different chemical composition and activity. In terms of volume, they usually represent the largest part of the nuclear power plant's radioactive waste. Some liquid wastes can be discharged outside the premises of the nuclear power plant after decontamination below the permissible level. Decontaminated wastewater with an activity above the permissible standard can be reused in the operation of a nuclear power plant after treatment by evaporation, ion exchange or chemical treatment. Such waters include, for example, wastewater from laundries and drainage water from pipe systems and equipment.

During the processing of reusable radioactive liquid waste, non-reusable wastewater is produced as secondary waste. Sometimes this waste is referred to as semi-liquid. These are concentrates and sludges that cannot be discharged from the power plant premises, while the majority of them are low-level and intermediate-level waste. A small part is made up of highly active concentrated residues. Before placing this type of waste in a deep repository, it is necessary to modify its form through various processes, such as cementation, bituminization and vitrification).

A relatively large part of the waste produced in the nuclear power plant consists of gaseous radioactive waste. It is discharged from the ventilation chimney after treatment and monitoring. Its quantity and composition are primarily determined by the activity from the exhaust systems of technological equipment and operating rooms. Due to the short half-life of the contained radionuclides and relatively low biological efficiency compared to other types of waste, gaseous radioactive wastes represent a minor technological problem in their treatment and processing.

### IV. INCINERATION OF RADIOACTIVE WASTE

Depending on the type and properties of radioactive waste, there are several technological processes for its effective disposal. These processes include, for example, bituminization, vitrification and incineration. During the incineration process, combustible solid and liquid radioactive waste is disposed of. Incineration is not a waste-free technology. The primary goal of incinerating radioactive waste is to reduce its volume.

The diagram of the low-level waste treatment process using incineration is shown in fig. 1. After initial sorting, solid radioactive waste is brought in barrels for further sorting. After weighing and measuring the activity of radionuclides, compactable solid waste is compacted through a high-pressure press in barrels, which are then stored in fiber concrete containers. Combustible wastes are brought to the premises of the incinerator using transport devices designed for this purpose in gradually dosed quantities. In addition to solid fuel, liquid radioactive waste with oil is dosed into the incinerator to support combustion along with ionex.

Incineration takes place in the main incineration furnace at temperatures in the range of 750-950 °C. The generated radioactive gases are combusted in the combustion chamber at a temperature of 1000 °C. After cooling, the remaining gases are cleaned and filtered in special equipment. The ash produced by combustion has different grain sizes and compositions. It is fixed in the



strengthening matrix by adding paraffin. The spent water used for flue gas cleaning is after treatment used for the preparation of cement grout.

The cementation device enables treatment of solid radioactive wastes, or of radioactive wastes fixed in the matrix, with a cement grout mixed with concentrates, sludge and saturated sorbents into a fiber concrete container, which is sealed after filling and stored in the dispatch warehouse for a specified period of time for aging.

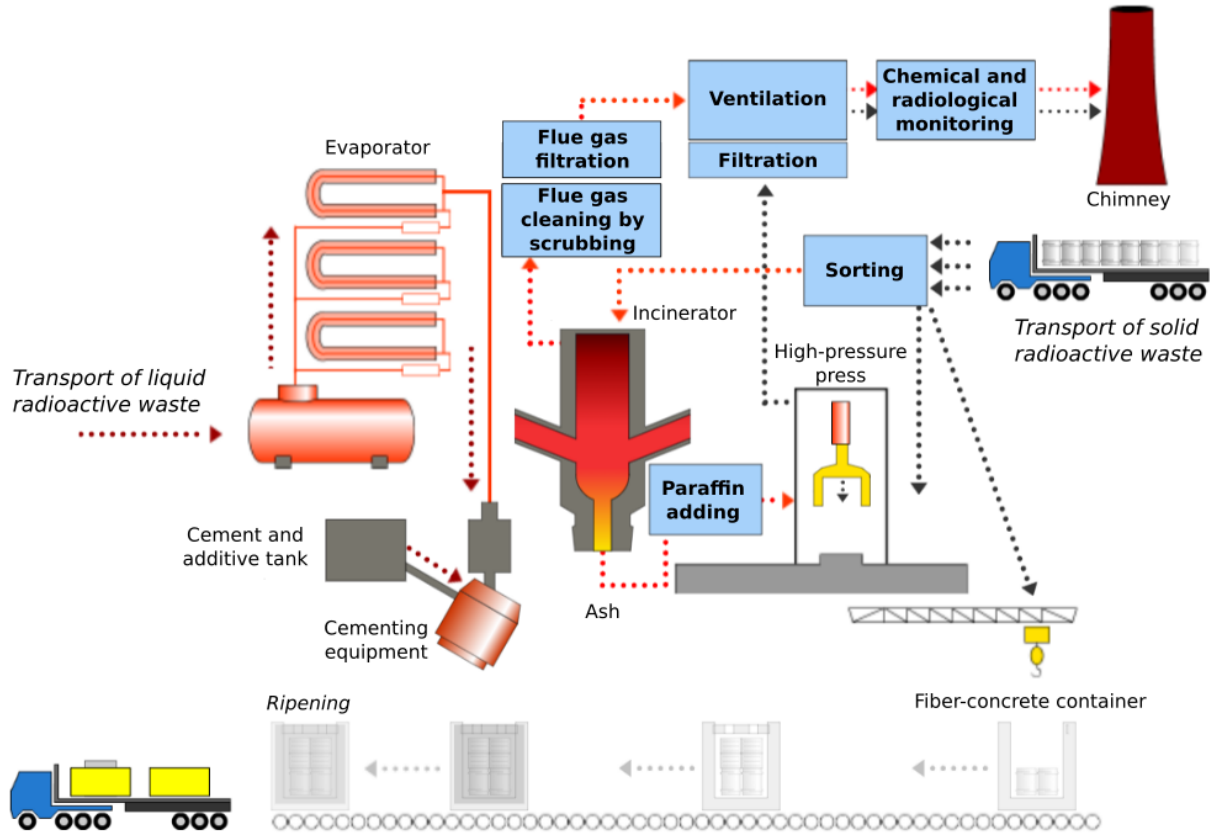


**FIGURE 1: Diagram of the low-level waste treatment process**

**V. DETERMINATION OF THE MASS FLOW OF COOLING WATER**

An important role in the incineration process has the feeder of liquid radioactive waste with ionex, which brings them into the premises of the main incinerator (Fig. 2). To support combustion, heating gas is supplied together with liquid waste. Foam serves as a transport medium for ionex.

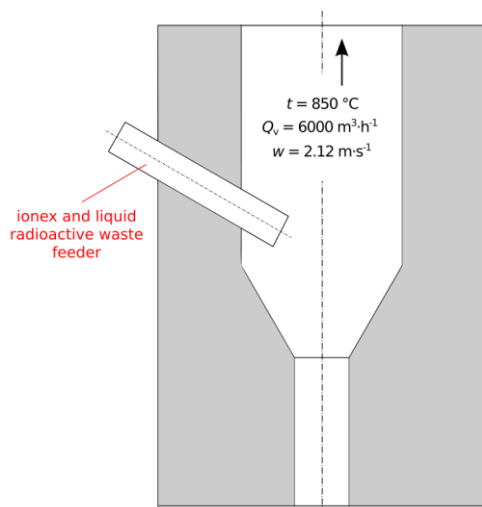


**FIGURE 2: Location of the feeder in the incinerator premises**

Ionex has a certain range of working temperatures, and when the maximum temperature is exceeded, ionex is baked on the walls of the feeder pipe. This ultimately disrupts the continuity of the combustion process. It is therefore necessary to avoid exceeding the maximum permitted temperature by effective cooling.

When determining the properties of the flue gas using the software, the theoretical composition of the flue gas of the waste mixture was used (Table 1).

**TABLE 1**  
**THEORETICAL COMPOSITION OF THE FLUE GAS OF THE WASTE MIXTURE**

$O_{2min} (m^3 \cdot kg^{-1})$	29.3813	$O_{2min} (\% \cdot kg^{-1})$	12.1853
$V_{CO_2} (m^3 \cdot kg^{-1})$	21.9667	$V_{CO_2} (\% \cdot kg^{-1})$	9.1103
$V_{SO_2} (m^3 \cdot kg^{-1})$	0.04885	$V_{SO_2} (\% \cdot kg^{-1})$	0.0203
$V_{H_2O} (m^3 \cdot kg^{-1})$	14.5678	$V_{H_2O} (\% \cdot kg^{-1})$	6.0417
$V_{N_2} (m^3 \cdot kg^{-1})$	177.8494	$V_{N_2} (\% \cdot kg^{-1})$	73.7594
$V_{O_2} (m^3 \cdot kg^{-1})$	26.688	$V_{O_2} (\% \cdot kg^{-1})$	11.0683

Based on the data from Table 1, the properties of the flue gas (Table 2) necessary for further calculations were determined.

**TABLE 2**  
**PROPERTIES OF THE FLUE GAS OF THE WASTE MIXTURE**

<b>Kinematic viscosity <math>\nu (m^2 \cdot s^{-1})</math></b>	$74.14562 \cdot 10^{-6}$
<b>Dynamic viscosity <math>\eta (Pa \cdot s)</math></b>	34.29172
<b>Density <math>\rho (kg \cdot m^{-3})</math></b>	0.46249
<b>Prandtl criterion <math>Pr</math></b>	0.7097

The calculation of the heat transfer coefficient  $\alpha$  was carried out using the criterion equations for the transverse flow around the pipe at an angle. To calculate the Reynolds criterion  $Re$ , it was necessary to determine the characteristic dimension  $l$ :

$$l = \frac{\pi \cdot d}{2} = \frac{\pi}{2} \cdot 0.202 = 0.317 \text{ (m)} \quad (1)$$

Where  $d$  is the outer diameter of the pipe (m).

Then the following equation is used to calculate  $Re$ :

$$Re = \frac{\omega \cdot l}{\nu} = \frac{2.12 \cdot 0.317}{74.14562 \cdot 10^{-6}} = 9063.79 \quad (2)$$

Where  $\omega$  is the fluid velocity ( $m \cdot s^{-1}$ ),  $l$  is the characteristic dimension (m) and  $\nu$  is the kinematic viscosity ( $m^2 \cdot s^{-1}$ ).

The calculation of the Nusselt criterion  $Nu$  is expressed by equations 3 – 8:

$$Nu_{l,lam} = 0.664 \cdot \sqrt{Re} \cdot \sqrt[3]{Pr} = 0.664 \cdot \sqrt{9063.79} \cdot \sqrt[3]{0.7097} = 56.387 \quad (3)$$

$$Nu_{l,turb} = \frac{0.037 \cdot Re^{0.8} \cdot Pr}{1 + 2.443 \cdot Re^{-0.1} \cdot (Pr^{\frac{2}{3}} - 1)} = \frac{0.037 \cdot 9063.79^{0.8} \cdot 0.7097}{1 + 2.443 \cdot 9063.79^{-0.1} \cdot (0.7097^{\frac{2}{3}} - 1)} = 48.131 \quad (4)$$

$$Nu_{l,0} = 0.3 + \sqrt{Nu_{l,lam}^2 + Nu_{l,turb}^2} = 0.3 + \sqrt{56.387^2 + 48.131^2} = 74.436 \quad (5)$$

$$K = \left( \frac{T_b}{T_w} \right)^{0.12} = \left( \frac{1123.15 + 323.15}{323.15} \right)^{0.12} = 1.101 \quad (6)$$

Where  $T_b$  is the boundary layer temperature (K) a  $T_w$  is the wall temperature (K).

$$Nu_l = Nu_{l,0} \cdot K = 74.436 \cdot 1.101 = 81.954 \quad (7)$$

During flow around the pipe, we consider the angle of impact of the flue gases on the feeder to be  $45^\circ$ . The ratio  $Nu_{l,\varphi}/Nu_l = 0.805$  corresponds to this angle.

$$Nu_{l,\varphi} = 0.805 \cdot Nu_l = 0.805 \cdot 81.954 = 65.973 \quad (8)$$

Then equations 9 – 12 apply to the calculation of the convective, radiation and overall heat transfer coefficient:

$$S = \pi \frac{d^2}{2} + \pi \cdot d \cdot L = \pi \frac{0.202^2}{2} + \pi \cdot 0.202 \cdot 1.56 = 1.054 \text{ (m)} \quad (9)$$

$$\alpha_c = \frac{Nu_{l,\varphi} \cdot \lambda}{l} = \frac{65.973 \cdot 0.069}{0.317} = 14.36 \text{ (W} \cdot \text{m}^{-2} \cdot \text{K}^{-1}) \quad (10)$$

$$\alpha_r = \frac{\varepsilon \cdot \sigma \cdot S (T_a^4 - T_m^4)}{S (T_a - T_m)} = \frac{0.9 \cdot 5.6704 \cdot 10^{-8} \cdot 1.054 \cdot (1123.15^4 - 323.15^4)}{1.054 \cdot (1123.15 - 323.15)} = 100.82 \text{ (W} \cdot \text{m}^{-2} \cdot \text{K}^{-1}) \quad (11)$$

$$\alpha_o = \alpha_c + \alpha_r = 14.36 + 100.82 = 115.18 \text{ (W} \cdot \text{m}^{-2} \cdot \text{K}^{-1}) \quad (12)$$

where  $S$  is the surface of the body ( $\text{m}^2$ ),  $L$  is the pipe length (m),  $\alpha_c$  is the convective heat transfer coefficient ( $\text{W} \cdot \text{m}^{-2} \cdot \text{K}^{-1}$ ),  $\alpha_r$  is the radiation heat transfer coefficient ( $\text{W} \cdot \text{m}^{-2} \cdot \text{K}^{-1}$ ),  $\alpha_o$  is the overall heat transfer ( $\text{W} \cdot \text{m}^{-2} \cdot \text{K}^{-1}$ ),  $\lambda$  is the thermal conductivity coefficient ( $\text{W} \cdot \text{m}^{-1} \cdot \text{K}^{-1}$ ),  $\varepsilon$  is the body emissivity (-),  $\sigma$  is the Stefan–Boltzmann constant ( $\text{W} \cdot \text{m}^{-2} \cdot \text{K}^{-4}$ ),  $T_a$  the ambient temperature (K) and  $T_m$  is the medium temperature inside the body (K).

After determining the convection and radiation coefficient of heat transfer, it is possible to determine the heat flow by convection  $P_c$  and radiation  $P_s$ :

$$P_c = \alpha_c \cdot S (T_a - T_m) = 14.36 \cdot 1.054 \cdot (1123.15 - 323.15) = 12\,108.3 \text{ (W)} \quad (13)$$

$$P_r = \varepsilon \cdot \sigma \cdot S (T_a^4 - T_m^4) = 0.9 \cdot 5.6704 \cdot 10^{-8} \cdot 1.054 \cdot (1123.15^4 - 323.15^4) = 85\,594.8 \text{ (W)} \quad (14)$$

The last step after the calculation of the total heat flow by radiation and convection is the determination of the mass flow of water  $Q_m$  required for effective cooling of the feeder. Treated river water with an average temperature of  $20^\circ\text{C}$  serves as a coolant.

$$Q_m = \frac{P_c + P_r}{c_{p,H_2O} (T_2 - T_1)} = \frac{12\,108.3 + 85\,594.8}{4180 \cdot (323.15 - 293.15)} = 0.779 \text{ (kg} \cdot \text{s}^{-1}) \quad (15)$$

Where  $c_{p,H_2O}$  is the specific heat capacity of water ( $\text{J} \cdot \text{kg}^{-1} \cdot \text{K}^{-1}$ ),  $T_1$  is the water temperature at the entrance to the body (K) and  $T_2$  is the water temperature at the outlet of the body (K).

## VI. CONCLUSION

Although the positive benefits of nuclear energy for mankind are undeniable, for its safe operation, proper management of the waste generated during the production of electricity is essential. The disposal of radioactive waste is possible by various methods that are constantly being developed and made more efficient. Using the criterion equations, it is possible to determine the heat transfer coefficients and subsequently determine the heat flow by convection and radiation during the cooling process of the liquid radioactive waste feeder to the incinerator. Knowing the total heat flow is essential for the next steps in the process of optimizing the feeder cooling through numerical simulations, which will be covered in Part II. In the calculations, the worst possible scenario was considered, when the cooling water reaches up to  $20^\circ\text{C}$ . When using cooling water at lower temperatures, it would be possible to consider a lower mass flow, which makes it possible to achieve financial savings in the area of treatment and transport of cooling water.

## ACKNOWLEDGEMENTS

This paper was written with financial support from the VEGA granting agency within the projects no. 1/0224/23 and no. 1/0532/22, from the KEGA granting agency within the project no. 012TUKE-4/2022 and with financial support from the APVV granting agency within the projects no. APVV-15-0202, no. APVV-20-0205 and no. APVV-21-0274.

## REFERENCES

- [1] Ch. W. Forsberg, "Radioactive Wastes". In: *Encyclopedia of Physical Science and Technology* (Third Edition). Academic Press, 2003. Pages 643-659, ISBN 9780122274107. DOI: <<https://doi.org/10.1016/B0-12-227410-5/00642-6>>

- [2] H. W. Wang, M. Q. Chen, K. Fu, S. H. Wei, X. B. Zhong, "Evaluation on migration and transformation of trace nuclides in thermal degradation for low-level radioactive waste". In: *Journal of Analytical and Applied Pyrolysis*, 2022. Volume 161, 105420, ISSN 0165-2370. DOI: <<https://doi.org/10.1016/j.jaap.2021.105420>>
- [3] VDI Heat Atlas, GVC, Düsseldorf, 1993. ISBN 978-3-540-79999-3.
- [4] JAVYS, "Bohunické spracovateľské centrum RAO" [online]. Available at: <<https://www.javys.sk/sk/jadrove-zariadenia/technologie-spracovania-a-upravy-rao/bohunicke-spracovateleske-centrum-rao>> [cit. 09-08-2023]
- [5] J. Kumičák, "Heat and mass transfer". Košice, TU, 2003. 67 pages. ISBN 80-7099-990.
- [6] V. Bauer, M. Šofranko, M. Stavníkovič, "Výskum multibariérového systému pre hlbinné ukládanie rádioaktívnych odpadov". In: *Acta Montanica Slovaca*, 2007. Volume 12, Issue 1, Pages 217-225.
- [7] K. R. Randive, P. Godbole, S. Jawadand, V. Chopra, M. L. Dora, S. J. Dhoble, "12 – Radioactive waste management in India: present status and future perspectives". In: *360-Degree Waste Management*, 2023. Volume 2, Pages 273-298. DOI: <<https://doi.org/10.1016/B978-0-323-90909-9.00005-8>>.

# Design of An Experimental Device for the Analysis of the Influence of Sound Waves on the CPU Cooling Process - Part I

Lukáš Tóth<sup>1\*</sup>, Romana Dobáková<sup>2</sup>

Department of Energy Engineering, Faculty of Mechanical Engineering, Technical University of Košice, Slovakia

\*Corresponding Author

Received: 07 October 2023/ Revised: 16 October 2023/ Accepted: 23 October 2023/ Published: 31-10-2023

Copyright © 2023 International Journal of Engineering Research and Science

This is an Open-Access article distributed under the terms of the Creative Commons Attribution Non-Commercial License (<https://creativecommons.org/licenses/by-nc/4.0>) which permits unrestricted Non-commercial use, distribution, and reproduction in any medium, provided the original work is properly cited.

**Abstract**— *The article discusses the design and preparation of the experimental equipment for the analysis of the cooling power of air cooling at various operating parameters. The basis of the article is an analysis of the needs and maximum thermal output of the CPU. Subsequently, it presents the design of the experiment with the calibration requirements. It describes processes for creating a basic package of data as an initial point for experimental analysis and solving the problem of increasing the air-cooling efficiency using acoustic waves.*

**Keywords**— *CPU, TDP, Cooling Process.*

## I. INTRODUCTION

The increasing output of computer components such as CPU and graphics cards involve the need to increase the outputs of cooling devices, whose task is to remove the heat generated during the operation of the computational parts of the computer. The increase in the amount of the removed heat is associated with an increase in the size of the cooling units, whether it is water or air cooling. However, the expansion of cooling systems is limited by the size of the space defined by the outer casing of the computer. Current cooling units, primarily the water-cooling take up a significant space at the outer walls. Therefore, increasing the cooling efficiency of computational computer components is starting to come to the fore in connection with the effort to minimize space a modern computer should occupy and with miniaturization, lightening and at the same time increasing the output of portable computers. One of the biggest limitations of current laptops, which causes their lower output in comparison to desktop computers, is precisely their inability to cool the computational components as efficiently as in comparison to a desktop computer.

## II. THERMAL OUTPUTS OF CURRENT CPUS

Nowadays, the main indicator of the amount of necessary heat removed from the CPU – computational component, is the TDP value – Thermal Design Power, which, however, does not determine the maximum possible heat output of the CPU, but only the maximum heat output of the CPU during normal processes. During the processes that intentionally overload the CPU, there can be an increase in heat output, which needs to be dissipated from the surface to prevent any thermal damage to the cooled electrical components.

A significant problem is the TDP definition itself, since each manufacturer of the CPUs for computers defines individually, how this value is determined, and in some cases, the manufacturer has various definitions of TDP for different series of CPUs. As an example, we can use the TDP definitions of the two biggest manufacturers of CPU:

The AMD definition

- “TDP is the maximum current the CPU can draw at the factory voltage and frequency under the worst thermal conditions.”

- TDP Thermal Design Power. The thermal design power is the maximum power a processor can draw for a thermally significant period while running commercially useful software [1].
- TDP Thermal design power. A power consumption parameter that is used in conjunction with thermal specifications to design appropriate cooling solutions for the processor [2].

#### Intel definition

- From the CPU datasheet with the Northwood core: “The number in this column reflects a recommended point and does not indicate the maximum power that the CPU can emit under the worst conditions”.
- For the Prescott cores it has a different definition: “TDP should be used as a target for cooling design for a given CPU. TDP is not the maximum thermal output the CPU can emit”.
- From Intel support: “TDP stands for Thermal Design Power, in watts, and refers to the power consumption under the maximum theoretical load. Power consumption is less than TDP under lower loads. The TDP is the maximum power that one should be designing the system for. This ensures operation to published specs under the maximum theoretical workload” [3].

Because of the reason given by inhomogeneity and non-uniform definition of TDP it is only possible to determine that TDP can be used for an approximate determination of the thermal output of the given CPU. Comparing, for instance, CPUs from AMD and Intel companies (or even any other CPU series from the same company) using TDP is simply not possible, due to the different interpretation of TDP by both companies. TDP also does not say anything about CPU consumption at low load (office work, ...), which is, for example, much more important for laptops than consumption at full load [4].

For the comparison in labelling and TDP values, a table was compiled with the TDP values of common types of CPUs used in desktop computers.

**TABLE 1**  
**PARAMETERS OF CURRENT CPU**

Name	Number of cores	Frequency	Production technology	Number of fibres	TDP (W)
AMD Ryzen Threadripper PRO 5995WX	64	2.7 GHz	7 nm	128	280
Intel Core i9-13900KS	24	3 GHz	10 nm	32	253
AMD Ryzen 9 7950X3D	16	4.2 GHz	5 nm	32	120
Intel Core i9-11900K	8	3.5 GHz	14 nm	16	125
Intel Core i7-13700F	16	2.1 GHz	7 nm	24	219
Intel Core i5-13600KF	14	3.5 GHz	10 nm	20	181
AMD Ryzen 9 5900X	12	3.7 GHz	7 nm	24	105
AMD Ryzen Threadripper PRO 5965WX	24	3.8 GHz	7 nm	64	280

As can be seen in Table 1, it is not possible to establish any precise connection between the number of cores, fibres, and the thermal output of the CPU. The only thing that can be said with certainty is that with the increasing number of cores and with the increasing computational power, the heat output that needs to be removed from the surface of the CPU also increases. However, this value is not directly proportional, as seen on the example of CPU from AMD company, namely AMD Ryzen

Threadripper PRO 5965WX and AMD Ryzen Threadripper PRO 5995WX, when both have the same TDP, but in the case of the 5965WX version, the number of cores and of the fibres is half of that of the 5995WX (tab. 1).

### III. DESIGN OF THE EXPERIMENT

Since it's not possible to reach a general conclusion connecting the basic parameters of the CPU with its thermal power, which is caused both by different TDP definitions and also different working conditions of the CPU, it is necessary to create certain generalization of the thermal output that will be considered the maximum possible during the experiments. Due to this, an air cooler, for which the manufacturer indicates the maximum value of the heat output that this cooler can remove to the surrounding environment under maximum operating conditions, was chosen for the CPU. Based on this data, the maximum heat output for the simulated CPU was also chosen, since even in the case of a real CPU, there would be no greater heat dissipation than the maximum value given by the cooler manufacturer.



FIGURE 1: Deepcool AG200 [5]

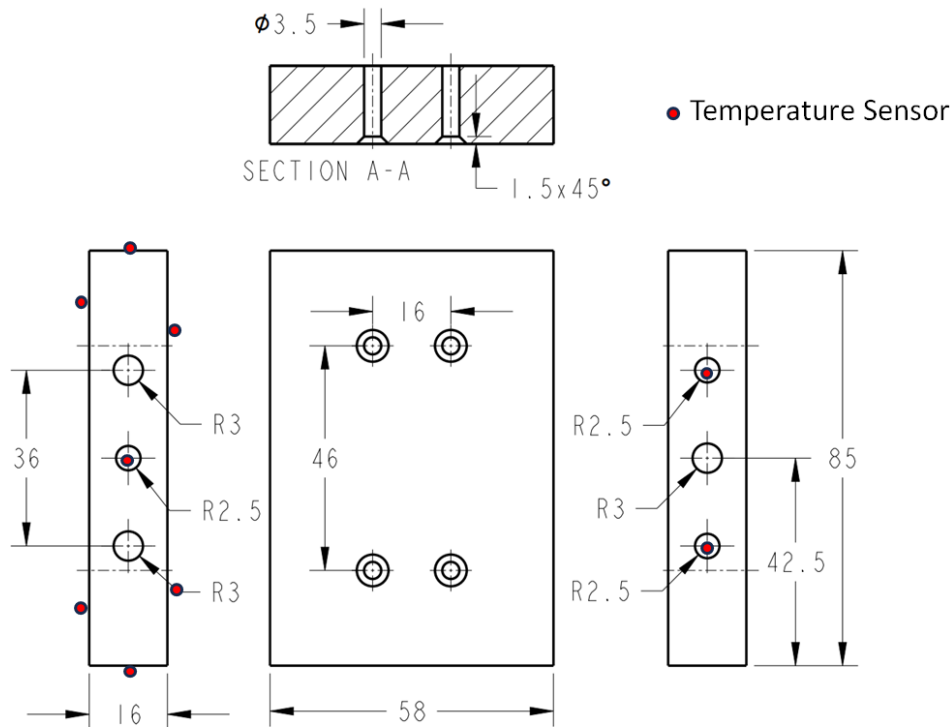
For the experiment and determination of operating parameters, a commercially available model of air cooling with 2 heat pipes - DeepCool AG200, whose basic information is described in Table 2, was chosen.

TABLE 2  
BASIC PARAMETERS OF THE DEEPCOOL AG200 [5]

Width	94 (mm)
Height	133 (mm)
Depth	66 (mm)
Number of heat pipes	2
Fan diameter	92 (mm)
Air flow	36.75 CFM
	62.44 (m <sup>3</sup> ·h <sup>-1</sup> )
Maximum loudness	30.5 (dB)
Maximum speed	3050 RPM
Minimum speed	500 RPM
Weight	304 (g)
Maximum TDP	100 (W)

As a CPU simulation with a uniform temperature field distribution, an aluminium block was used, with dimensions of 58, 85 a 16 mm, in which 3 heating modules, each with the maximum power of 50W and diameter of  $\phi 6$  mm, were placed. The maximum heat output of the simulated CPU was 150W, which is 50W more than the manufacturer's maximum TDP for the cooler, which is 100W. 3 NTC 10K thermometers with a diameter of  $\phi 5$  mm were also placed in the body, and 6 DS18B20 and SMT172R16A thermometers were installed on the surface of the device. The task of the given number of thermometers is to ensure the scanning of the distribution of the temperature field within the aluminium block and to determine the maximum temperature reached during the cooling process. The distribution of the heating modules is shown on the Figure 2.

Thermometers SMT172R16A were placed on the sidewalls of the aluminium block, temperature sensors DS18B20 were placed on the top and bottom of the aluminium block.



**FIGURE 2: Parameters of the CPU simulator with the indication of the location of the temperature sensors**

The entire aluminium block is isolated with rubber insulation with the width of 10 mm, on which there is a reflective aluminium layer.

Another set of thermometers together with an anemometer is in the area of the fan and cooler plates, where they record the distribution of the temperature field along the layers of the cooling plates, the air temperature before entering the fan and after exiting the area of the cooling plates. The air coming out of the cooling plates travels into a conical-shaped collector, at the end of which there is a propeller anemometer for determining the amount of air passing through the body of the cooler at different power settings of the fan.

The basis of the calibration experiments was the creation of a database determining the cooling power of the CPU air cooler under certain output conditions given by fan revolution speed and ambient temperature. With the help of heating modules, where the heat output was increased and decreased during each series of measurements, the temperature of the aluminium block simulating the CPU was stabilized. After the stabilization of the aluminium block, the amount of heat supplied by the heating modules equals the cooling output of the cooler under given output conditions. Thanks to the knowledge of the voltage and the current supplied to the heating modules, it is possible to determine relatively precisely the cooling power for the given output parameters of the cooler determined by the fan speed and the ambient temperature. The regulation of the fan revolution speed, along with the scanning of the current value of the fan rotation speed, was carried out through the Arduino MEGA microcontroller. The set speed range was set from the lowest possible, given by the manufacturer at a value of 500 rpm to a maximum of 3000 rpm. The fan speed was increased by 500 rpm for each series of measurements. At the same time, the Arduino serves as a bus for the values of the measured temperatures from the CPU simulator and the distribution of the temperature field within the cooler.

#### IV. SENSOR CALIBRATION

Since NTC sensors are used to measure temperatures, in which their resistance changes along with the change in temperature, it is necessary to calibrate each sensor due to small inaccuracies, which may occur during the production process. These inaccuracies may subsequently cause measurement deviations in the range of tenths to several degrees. Such deviations are unacceptable but can be reduced with calibrating the sensors. To calibrate the sensors, a water bath with a precisely defined temperature, an integrated temperature sensor and an external Alhorn PT 100 thermometer connected to the ALMEMO 2890-



9 data bus were used. Multiple check ensures an increase in the accuracy of sensor calibration. The water bath was chosen due to its easy handling and the possibility to change temperature, which is the same throughout the entire volume of the liquid, within degrees in the range of measurement from 25 °C - room temperature in the laboratory, up to a temperature of 70 °C, which we consider to be the maximum for use CPU.

Each sensor was labelled and in Table 3 we can see the example of how the resistance of the thermistors changed with the change in the temperature. As can be seen in Picture 3, there is no linear change in the resistance of the thermistors, but there is a curve, and the curve is partially different for each thermistor. Such differences occur due to imprecise resistance values and production deviations in the production of thermistors.

**TABLE 3**  
**DIGITAL SIGNALS SENT BY SENSORS T1-T4 AT DIFFERENT TEMPERATURE**

	Temperature (°C)							
	35	40	45	50	55	60	65	70
T1	413	364	321	291	268	252	240	204
T2	412	363	320	286	263	245	231	203
T3	412	363	317	280	247	220	197	174
T4	407	358	312	272	235	202	174	157

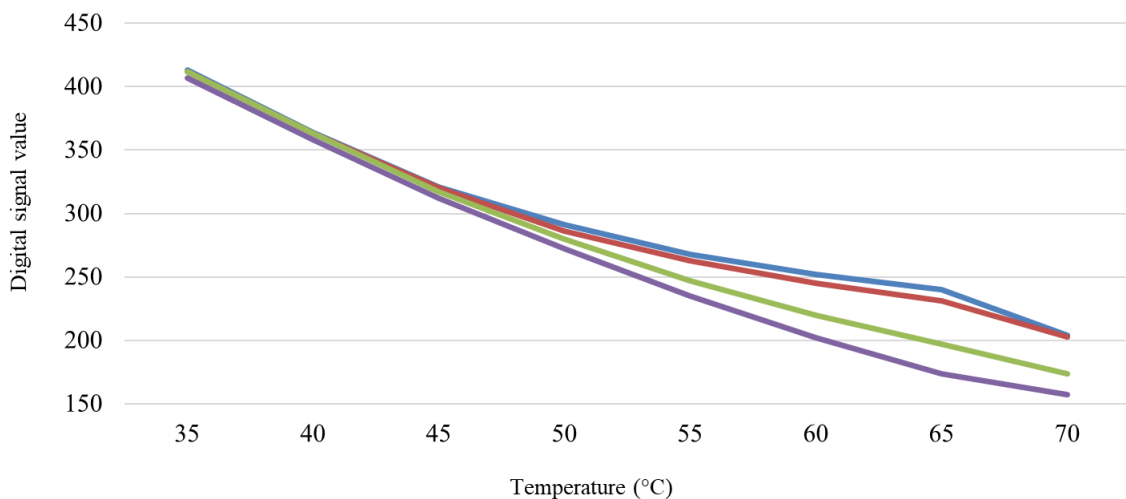


**FIGURE 3: Graphic representation of the change in digital signal from the T1-T4 sensors during the temperature change**

Measuring of changes in the value of the 10K thermistors was recorded using an Arduino MEGA microcontroller on analog inputs that can record a signal in the range of 0-1024. A prescribed resistance was placed across the thermistor as shown in Figure 4.

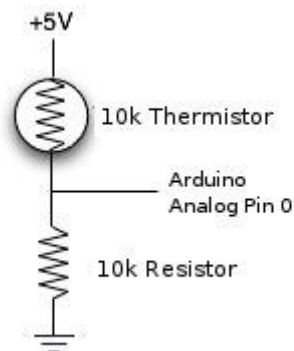


**FIGURE 4: Thermistor connection diagram**

The calibration of the digital sensors took place under the same conditions. The accuracy of selected temperature sensors varies in the case of DS18B20 in the range of  $\pm 0,5^{\circ}\text{C}$ . Because of this, several sensors are placed in different places within the aluminium block and the temperature of the block is given as the average measured value of these sensors in a stable state, when there was no temperature change. We connected all DS18B20 sensors using a common 1-Wire bus to the Arduino Mega microcontroller. Thanks to the unique 64-bit identifier of each DS18B20 sensor, individual sensors can be directly addressed, which allows us to assign them to specific positions. The disadvantage of such connection is a slower loading of data since all temperature sensors share one common data bus. In the case of a stable state, it's not necessary to carry out a series of measurements following in short time intervals; therefore, this method of connection was chosen as more economical. The advantage is also the reduction of the number of conductors passing through the aluminium block insulation, which also reduces the amount of heat dissipated to the surroundings.

## V. CONCLUSION

The article described the design of a system for the analysis of increasing the efficiency of CPU cooling using an air cooler. Calibration of the temperature sensors distributed within the aluminium block simulating the CPU was carried out. The calibration was also performed on the thermistors located between the ribs of the air cooler and at the inlet and outlet of the cooling air.

The basic calibration and creation of an initial comparison data package of the cooling power of the air cooler at different operating parameters will be described in the second part of this article.

## ACKNOWLEDGEMENTS

This paper was written with the financial support from the VEGA granting agency within the Projects No. 1/0224/23 and No. 1/0532/22, from the KEGA granting agency within the Project No. 012TUKE-4/2022, and with the financial support from the APVV granting agency within the Projects No. APVV-15-0202, APVV-20-0205 and APVV-21-0274.

## REFERENCES

- [1] AMD NPT Family 0Fh Desktop Processor Power and Thermal Data Sheet. Available on <<https://www.amd.com/content/dam/amd/en/documents/archived-tech-docs/datasheets/33954.pdf>>.
- [2] BIOS and Kernel Developer's Guide (BKDG) for AMD Family 15h Models 30h-3Fh Processors. Available on <[https://www.amd.com/content/dam/amd/en/documents/archived-tech-docs/programmer-references/49125\\_15h\\_Models\\_30h-3Fh\\_BKDG.pdf](https://www.amd.com/content/dam/amd/en/documents/archived-tech-docs/programmer-references/49125_15h_Models_30h-3Fh_BKDG.pdf)>.
- [3] INTEL. Thermal Design Power (TDP) in Intel® Processors. Available on <<https://www.intel.com/content/www/us/en/support/articles/000055611/processors.html>>.
- [4] Garmatyuk, S.: *Testing Thermal Throttling in Pentium 4 CPUs with Northwood and Prescott cores*. Ixbtlabs (2004), Available on <<http://ixbtlabs.com/articles2/p4-throttling/>>.
- [5] DEEPCOOL. Available on <<https://www.deepcool.com/products/Cooling/cpuaircoolers/AG200-Single-Tower-CPU-Cooler-1700-AM5/2022/16203.shtml>>.
- [6] Cheng, C.C., Chang, P.C., Li, H.C., Hsu, F.I.: *Design of a single-phase immersion cooling system through experimental and numerical analysis*. International Journal of Heat and Mass Transfer. 160 (2020), 120203.
- [7] Liang, K., Li, Z., Chen, M., Jiang, H.: *Comparisons between heat pipe, thermoelectric system, and vapour compression refrigeration system for electronics cooling*. Applied Thermal Engineering. 146 (2019), p. 260-267
- [8] Qiu, D., Cao, L., Wang, Q., Hou, F., Wang, X.: *Experimental and numerical study of 3D stacked dies under forced air cooling and water immersion cooling*. Microelectronics Reliability. 74 (2017), p. 34-43.

# Device for Researching the Cooling Intensity of Flowing Media

Mária Čarnogurská<sup>1\*</sup>, Miroslav Příhoda<sup>2</sup>, Tomáš Brestovič<sup>3</sup>

<sup>1,3</sup>Department of Energy Engineering, Faculty of Mechanical Engineering, Technical University of Košice, 042 00 Košice, Slovak Republic

<sup>2</sup>Department of Thermal Engineering, Faculty of Materials Science and Technology, VSB –Technical University of Ostrava, 708 33 Ostrava-Poruba, Czech Republic

\*Corresponding Author

Received: 07 October 2023/ Revised: 19 October 2023/ Accepted: 24 October 2023/ Published: 31-10-2023

Copyright © 2023 International Journal of Engineering Research and Science

This is an Open-Access article distributed under the terms of the Creative Commons Attribution

Non-Commercial License (<https://creativecommons.org/licenses/by-nc/4.0>) which permits unrestricted

Non-commercial use, distribution, and reproduction in any medium, provided the original work is properly cited.

**Abstract**— The article describes the construction of a device for researching the effect of air flow speed on the intensity of cooling of the medium that flows in the ribbed tubes of the cooler. The measure of cooling intensity is the overall heat transfer coefficient  $k$ . It is a model of a tubular heat exchanger in which horizontal and vertical movement of the individual tubes of the heat exchange surface is possible. The device will be used to obtain information about the influence of the arrangement of the heat exchange surface on the cooling performance of the exchanger. The measured values of the relevant quantities will be used as input data for the ANSYS CFX software. The software will allow to simulate the current ratios in the radiator tubes, the temperature fields along the length of the tubes and in the individual tubes of the exchanger arranged according to its height.

**Keywords**— Ribbed heat exchange surface, flow distributor, cooling capacity.

## I. INTRODUCTION

To achieve suitable transport conditions, tubular heat exchangers with a ribbed external heat exchange surface are used at compressor stations for cooling natural gas [1-4]. The transported natural gas is compressed to the required transport pressure at the compressor station, which causes an increase in its temperature. Since the increase in gas temperature causes an increase in the volume of transport gas, the quality of cooling becomes one of the transport priorities. By reducing the temperature, the mechanical stress on the gas pipeline pipes caused by the expansion of their material is also reduced, which positively affects the service life of the gas pipeline.

The device described in the article is intended to provide information on the possibility of intensifying the heat exchange when cooling natural gas during the operation of the cooler. Natural gas coolers have different cooling surfaces, which are characterized by different tube diameters, different tube wall thicknesses, different rib diameters, and different rib spacing. However, the most important thing is the way the tubes are arranged in the cooler. The pipes are placed in rows above each other in the so-called "alternate arrangement" (Fig. 1). The number of rows of tubes is different. Structurally, the individual rows create an arrangement of either crossed flow (Fig. 2) or current doubly crossed (Fig. 3).

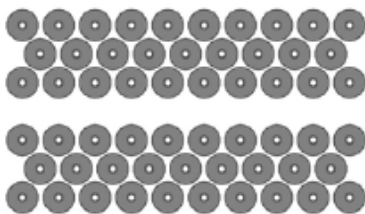


FIGURE 1: Pipe arrangement

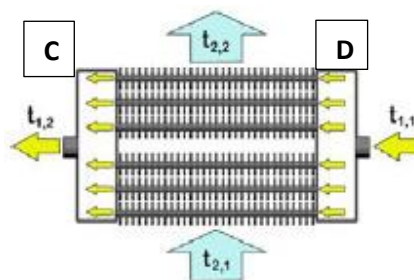


FIGURE 2: Cross current

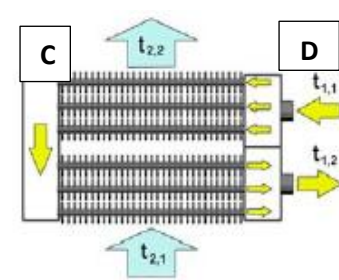


FIGURE 3: Double crossed current

In cross-flow the gas is fed to the distributor (D), from where it flows through all rows of cooling tubes in one direction. The tubes open into the collector (C), from where the gas is taken out of the cooler through the outlet pipes. With double cross current, the gas inlet and outlet to the cooler are on the same side of the cooler. In both cases, air is used to cool the gas, which is blown into the cooler by means of fans from the bottom up. Fan start-up is regulated depending on the desired output temperature.

## II. DESCRIPTION OF THE PROPOSED DEVICE

In laboratory conditions, water will be used instead of natural gas (safety point of view). The designed measuring device forms a closed circuit, which consists of a tubular heat exchanger (1) - a cooler, a fan placed under the cooler (2), a circulation pump (3), an accumulation flow water heater (4), a distributor (5), a collector (6), collecting tank (7) and connecting hoses (Fig. 4). The heat exchange surface is represented by the same pipework that is used to cool natural gas at the compressor station.

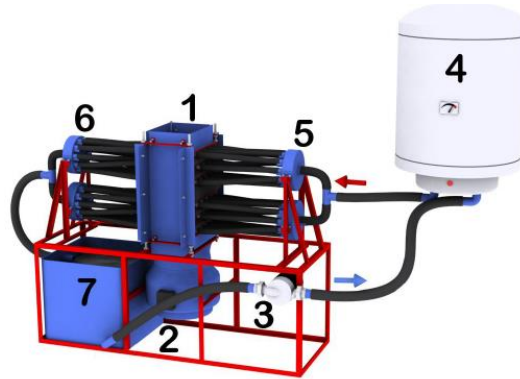


FIGURE 4: Assembly of measuring equipment

The main component of the measuring device is the tube exchanger, which is designed to ensure the greatest possible flexibility of the tube arrangement. The number of tubes placed one above the other can be up to 6, just like on a real natural gas cooler. The exchanger consists of ribbed pipes with a length of 2 m. The basic dimensions of the tube are shown in fig. 5. The individual pipes are fixed in the cooler structure in a staggered arrangement (Fig. 6). The device is currently prepared for measuring on tubes with the following dimensions: tube inner diameter  $d_1 = 25$  mm, tube outer diameter  $d_2 = 30$  mm, rib diameter  $d_r = 58$  mm, rib thickness  $h_r = 0.65$  mm, rib spacing  $b = 2.5$  mm.

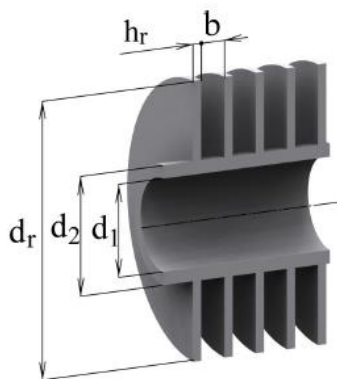


FIGURE 5: Basic dimensions of a pipe



FIGURE 6: Fixation of pipes in the structure of the device

The ends of the tubes are clamped in the measuring device between two steel bands, which are tightened using M 12 nuts threaded on threaded rods. The height adjustment of the pipes is ensured by the nuts on the underside of the steel belt. After setting the spacing between the tubes, the ends of the tubes are pressed against the steel strip using a nut. This will arrest the tubes. The tube block is then sheathed on the outside. This creates a closed space for the cooling air supply (Fig. 7).

On the sides, the exchanger casing consists of sheet metal parts with the possibility of precise adjustment of the gap between the outer tube and the shell. From the sides of the water inlet to the exchanger, the space is sealed with rubber seals (Fig. 8).

The sheathed heat exchanger is mounted on an L-shaped profile steel support frame. A VKMS 315 fan with a maximum air flow rate of  $1,880 \text{ m}^3 \cdot \text{h}^{-1}$  is placed under the heat exchanger. Water entering and exiting the heat exchanger is ensured by a flow distributor - position 5 in Fig. 4. Distributors ensure uniform distribution of the flow to all pipes of the exchanger. The connection of the distributors depends on the way the water flows through the exchanger. In the case of crossed current, two distributors and 2 collectors connected according to Fig. 9. In case of doubly crossed current, one distributor and one collector will be used (Fig. 10). Water is provided in a closed circuit by a pump HGPA 25-8.0 U 180 with a maximum flow of  $12 \text{ m}^3 \cdot \text{h}^{-1}$  with three levels of regulation.

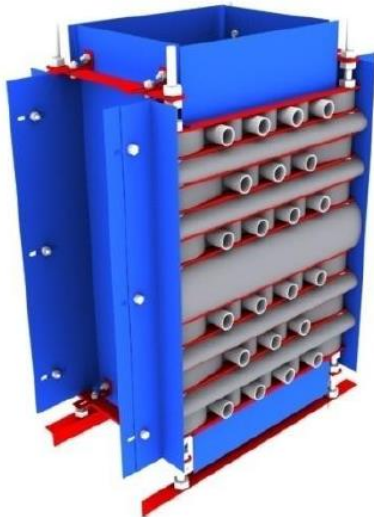


FIGURE 7: Exchanger with sheathing



FIGURE 8: Rubber seals on the inlet side of the exchanger



FIGURE 9: Diagram of connection of distributors for cross current



FIGURE 10: Wiring diagram of distributors for double cross current

### III. BASICS OF COOLING PERFORMANCE CALCULATION

The cooling performance of the cooler generally depends on several parameters. This is primarily about the type of cooled and cooling media and their thermal-physical properties, flow rates of both media, flow method through the cooler (convex, counter-flow, cross-flow), shape, size and material of the heat exchange surface, arrangement of pipes in the cooler, etc.

On the flowing water side, the basic relationship for the cooling power  $P$  can be given in the form:

$$P = \eta \cdot Q_{m,1} \cdot (i_{1,1} - i_{1,2}) = \eta \cdot Q_{m,1} \cdot c_{p,1} \cdot (t_{1,1} - t_{1,2}) = \eta \cdot \rho \cdot Q_{V,1} \cdot c_{p,1} \cdot \Delta t_1 \text{ (W)} \quad (1)$$

where  $i_{1,1}$  is the specific enthalpy of water at the inlet to the exchanger ( $\text{J} \cdot \text{kg}^{-1} \cdot \text{K}^{-1}$ ),

$i_{1,2}$  – specific enthalpy of water at the outlet of the exchanger ( $\text{J} \cdot \text{kg}^{-1} \cdot \text{K}^{-1}$ ),

$t$  – water temperature (°C); the indices are the same as for the designation of the specific enthalpy of water,

$c_{p,1}$  – specific heat capacity of water ( $\text{J}\cdot\text{kg}^{-1}\cdot\text{K}^{-1}$ ),

$Q_{m,1}$  – mass flow of water ( $\text{kg}\cdot\text{s}^{-1}$ ),

$\eta$  – coefficient respecting heat losses in the exchanger structure (1).

The total cooling performance of the exchanger can also be expressed from the heat balance:

$$P = k \cdot S_{\Sigma} \cdot \overline{\Delta t} \quad (\text{W}) \quad (2)$$

where  $k$  is the heat transfer coefficient referred to the outer surface area ( $\text{W}\cdot\text{m}^{-2}\cdot\text{K}^{-1}$ ),

$S_{\Sigma}$  – heat exchange surface on the outside ( $\text{m}^2$ ),

$\overline{\Delta t}$  – average temperature drop (K); in the case of cross-flow of heat-carrying media, it is determined as the mean logarithmic difference in the counter current exchanger, multiplied by the coefficient  $\psi$ . Its determination is stated in [5].

With known values of physical quantities, obtained from measurements on experimental equipment, the overall heat transfer coefficient  $k$  can be determined from the equation (3)

$$k = \frac{P}{S_{\Sigma} \cdot \overline{\Delta t}} = \frac{\eta \cdot \rho \cdot Q_{V,1} \cdot c_{p,1} \cdot \Delta t_1}{S_{\Sigma} \cdot \overline{\Delta t}} \quad (\text{W} \cdot \text{m}^{-2} \cdot \text{K}^{-1}) \quad (3)$$

The relationship (3) will allow obtaining the average value of the overall heat transfer coefficient  $k$  for various shaped heat exchange surfaces that will be placed in the designed experimental stand. To achieve a uniform distribution of the cooled medium in all tubes of the heat exchange surface, a "distributor" was designed (Fig. 11). The uniformity of the flow distribution was tested numerically, and the distributor was solved in the ANSYS CFX simulation tool (Fig. 12).

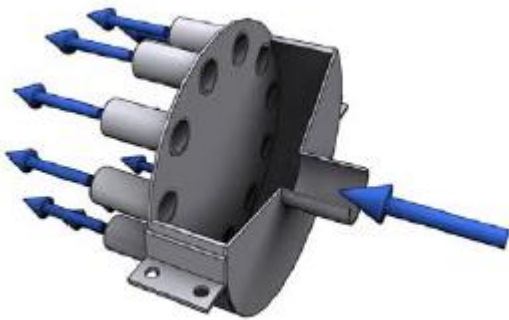


FIGURE 11: Cross-section of the flow distributor

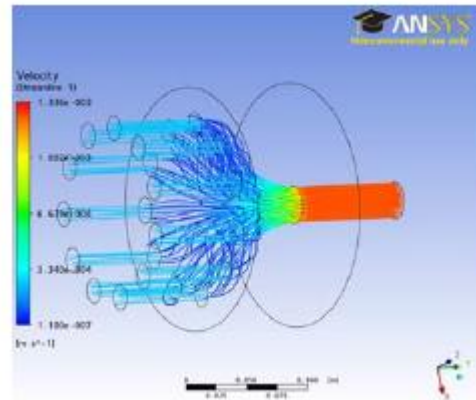


FIGURE 12: Simulation of water flow through the distributor

#### IV. DISCUSSION

When modeling the cooling performance, it is necessary to maintain the physical similarity between the model and the part. The heat dissipation to the surrounding air must be identical on the part and the model. In the model, water is used as the cooled liquid, in the real cooler it is compressed natural gas. It is necessary to ensure that the value of the heat transfer coefficient  $\alpha$  from the cooled medium to the inner surface of the tube has the same value on the part and the model. This results from the equality of the Nusselt criteria for the laboratory model and the real natural gas cooler. The flow of natural gas on a real cooler is turbulent. The heat transfer coefficient in the pipe is described by the criterion equation:

$$Nu = C \cdot Re^{0.8} \cdot Pr^{0.4}$$

where  $C$  is a coefficient (for gases,  $C$  is equal to 0.021; for liquids 0.023),

$Re$  – Reynolds criterion (1),

$Nu$  – Nusselt's criterion (1).

The same values of the factor  $\alpha$  on the part and the model will be achieved if the derived dependence in the form applies between the water flow rate  $w_w$  and the natural gas rate  $w_g$ :

$$w_w = w_g \cdot \left[ \frac{0.021}{0.023} \cdot \left( \frac{\nu_w}{\nu_g} \right)^{0.8} \cdot \left( \frac{Pr_g}{Pr_w} \right)^{0.4} \cdot \frac{\lambda_g}{\lambda_w} \right]^{1/0.8}$$

where  $\nu$  is the kinematic viscosity ( $\text{m}^2 \cdot \text{s}^{-1}$ ),

$\lambda$  – coefficient of thermal conductivity ( $\text{W} \cdot \text{m}^{-2} \cdot \text{K}^{-1}$ ),

$Pr$  – Prandtl's criterion (1);

Indexes "w" apply to water, indexes "g" to natural gas.

For the calculated speed of water circulation, it is necessary to finally check whether the water flow is also turbulent in the model. If, for example, at the compressor station, natural gas flows at a pressure of 7.35 MPa and a temperature of 60 °C through cooler tubes with an internal diameter of 25 mm at a speed of  $8.05 \text{ m} \cdot \text{s}^{-1}$ , then the coefficient  $\alpha$  has a value of  $1,632 \text{ W} \cdot \text{m}^{-2} \cdot \text{K}^{-1}$ . On the model through which 60°C warm water will flow, the same value of  $\alpha$  is reached at a speed of  $0.271 \text{ m} \cdot \text{s}^{-1}$ . The Reynolds criterion will be equal to 11,350, so the recirculation will be turbulent.

## V. CONCLUSION

The designed measuring device described in the article will make it possible to perform measurements both for crossed current and for double crossed current in various combinations of pipe arrangement (placed in rows one above the other and in alternating arrangement). The inlet (outlet) temperatures of both media will be measured just before the entrance (outlet) to the cooling space, as well as the media flow rates. Thermocouples will be used to measure the water temperature. By monitoring these temperatures, information will be obtained about the thermal performance of individual pipes, depending on their arrangement in the heat exchanger. Air temperatures will be measured just before the entrance (exit) to the cooling space and in the space between the pipes. The overall heat transfer coefficient  $k$  will be calculated from the measured values, which is a basic indicator of the intensity of heat exchange. The highest attainable overall heat transfer coefficient  $k$  will be sought through different combinations of pipe arrangement in the exchanger. The measured values will be compared with the numerical solution using FVM in the ANSYS CFX simulation tool.

## ACKNOWLEDGEMENTS

This paper was written with the financial support from the VEGA granting agency within the Projects No. 1/0224/23 and No. 1/0532/22, from the KEGA granting agency within the Project No. 012TUKE-4/2022 and Project SP 2023/34-FMT VŠB TUO.

## REFERENCES

- [1] M., Čarnogurská, M., Příhoda, T., Brestovič, Determination of deposit thickness in natural gas cooler based on the measurements of gas cooling degree. *Journal of Mechanical Science and Technology* 25 (11) (2011) pp. 2935-2941.
- [2] M., Čarnogurská, M., Příhoda, J., Václav, Comparison of pressure losses of clean and deposit-covered heat exchange surfaces of a natural gas cooler. *Acta Mechanica Slovaca* 18 (2) (2014) pp. 6-12.
- [3] M., Čarnogurská, M., Příhoda, J., M., Puškár, M., Fabián, R., Dobáková, M., Kubík, Measurement and mathematical modelling of heat loss in the pipe systems of a central heat distribution network. *Measurement* 94 (2016) pp. 806-811.
- [4] M., Čarnogurská, M., Příhoda, M., Lázár, N., Jasmínská, R., Gallik, M. Kubík, Measuring Selected Parameters of Polypropylene Fibre Heat Exchangers. *Strojnicki vestnik*, vol. 62, no. 6, (2016), pp.381-384.
- [5] M., Rédr, M., Příhoda. *Basics of Thermal Engineering*; SNTL: Praha, Czech, (1991) pp. 272-294. (In Czech).



**AD Publications**

**Sector-3, MP Nagar, Bikaner,  
Rajasthan, India**

**[www.adpublications.org](http://www.adpublications.org), [info@adpublications.org](mailto:info@adpublications.org)**